Noname manuscript No.
(will be inserted by the editor)

Large eddy simulations of CH_4 fire plumes

G. Maragkos · B. Merci

Received: date / Accepted: date

Abstract Large eddy simulations of large-scale CH_4 fire plumes (1.59-2.61 MW) with two different CFD packages, FireFOAM and FDS, are presented. It is investigated how the vorticity generation mechanism and puffing behavior of large-scale fire plumes differs from previously studied iso-thermal buoyant plumes of the same scale. In addition, the predictive capabilities of the turbulence and combustion models, currently used by the two CFD codes, to accurately capture the fire dynamics and the buoyancy-generated turbulence associated with large-scale fire plumes are evaluated. Results obtained with the two CFD codes, typically used for numerical simulations of fire safety applications, are also compared with respect to the average and rms velocities and temperatures, puffing frequencies, average flame heights and entrainment rates using experimental data and well-known correlations in literature. Furthermore, the importance of the applied reaction time scale model in combination with the Eddy Dissipation Model is examined. In particular, the influence of the considered mixing time scales in the predicted centerline temperatures is illustrated and used to explain the discrepancies between the two codes.

Keywords LES; fire plume; FireFOAM; FDS

1 Introduction

The study of fire plumes has received a lot of attention due to the great environmental impact and dangers often associated with them. More specifically, large-scale fire plumes, often encountered after natural fires and industrial accidents, can lead not only to severe air pollution due to the release of unburned hydrocarbons and soot into the atmosphere but can also trigger more severe cascading effects

G. Maragkos and B. Merci
Department of Flow, Heat and Combustion Mechanics, Ghent University,
St. Pietersnieuwstraat 41, B-9000 Ghent, Belgium
Tel.: +32 9264 32 90, Fax: +32 9264 35 75
E-mail: Georgios.Maragkos@UGent.be

involving explosions, causing huge losses of human lives and material properties. The use of Computational Fire Dynamics (CFD) has, nowadays, become an integral part of fire protection design of real life applications. Detailed knowledge of the behavior and the dynamics of large-scale fire plumes is, therefore, essential for fire safety engineers working on everyday life applications involving; fire detection, fire suppression and venting, design of smoke control systems, fire heating of structural elements of buildings or thermal radiation hazards [1,2]. CFD models can not only be used to evaluate the effectiveness of current or future fire protection systems but also to answer 'what if' questions and be used towards a cost-effective design without compromising fire safety in buildings. A deeper understanding of the capabilities and limitations of the available CFD codes available for performing numerical simulations of fire related applications will provide the fire safety engineers with the appropriate guidelines to carefully design and perform their CFD analysis when evaluating fire safety systems in buildings and industrial facilities.

The unsteady behavior and flow evolution of fire plumes of different scales, even though extensively studied in the past [3–6], still remains challenging due to the coupled physical processes involved, e.g., buoyancy-generated turbulence, combustion, thermal radiation and soot generation. Three regions are typically distinguished in fire plumes [7]: the flame region, close to the fire source, where continuous flames exist; the intermittent region where the flames strongly fluctuate exhibiting a characteristic puffing behavior; and the plume region, where combustion products are convected downstream and mixed with fresh air. What is typically encountered in large-scale fire plumes is a rapid transition of the flow, from laminar to fully turbulent, usually within a few inlet diameters from the fire source. Turbulence is greatly enhanced by strong buoyancy forces which result in a periodic shedding of large toroidal vortices (puffing behavior) near the base of the fire source. This puffing behavior is a key element in the fire dynamics of such plumes since it controls the air entrainment towards the reaction zone that will in turn influence the heat release rate, the composition of the combustion products and the soot generation.

The specific motivation of the present numerical study is three-fold: first, to study the dynamics and oscillatory behavior of large-scale fire plumes and examine how the vorticity generation mechanism and puffing frequency of such plumes differ from previously studied iso-thermal buoyant plumes [8,9] of the same size; second, to evaluate the predictive capabilities of the turbulence and combustion models, currently used in the fire community, of accurately capturing the fire dynamics and the buoyancy-generated turbulence associated with large-scale fire plumes; third, to apply two well-known CFD codes, typically used for numerical simulations of fire safety applications, and evaluate the simulation results of transient and mean flow dynamics of large-scale fire plumes against experimental data. The comparison of the two CFD packages is expected to be useful for fire safety engineers working on real-life applications of fire scenarios. As such, Large Eddy Simulations (LES) of 1 m in diameter CH_4 fire plumes are conducted with FireFOAM (version 2.2.x) and the Fire Dynamics Simulator (FDS) (version 6.1.2) and the numerical results are compared against experimental data and well-known correlations in literature.

It is worth noting, however, that it is not the authors' intention to directly compare the two CFD codes at hand, e.g., use identical numerical set-ups and modeling choices in the simulations, since such an attempt would not be possible due to limitations and differences of available models in each software. Given the

small differences in the modeling options employed in the two codes, this study aims at illustrating the potential of each software separately by comparing the numerical results with experimental data and correlations available in literature using the best available model options in each code. The work presented in the paper aims to focus on the strengths of each code as they stand but also to report their weaknesses so as to improve their models and, hence, their predictive capabilities. The present study is a significant extension of the previously conducted numerical study by Maragkos et al. [10], incorporating improvements in the selected physical models and a more detailed analysis. Within this mindset, the present paper also aims at expanding the work on small-scale CH_4 fire plumes, previously performed by Wang et al. [11] with FireFOAM (version 1.6) to large-scale CH_4 fire plumes.

2 Experimental case

Comparisons are made to the experiments performed in the Fire Laboratory for Accreditation of Modeling by Experiment (FLAME) facility at Sandia National Laboratories in Albuquerque, New Mexico, reported by Tieszen et al. [12,13]. The facility is a 6.1 m cubical enclosure with a 2.4 chimney located on the top of the chamber. The fire source, 1 m in diameter, is placed in the middle of the facility, positioned 2.45 m above the floor and is surrounded by a 0.51 m wide steel floor (ground plane). Particle Image Velocimetry (PIV) was used for velocity field measurements of CH_4 fire plumes with heat release rates ranging from 1.59 to 2.61 MW. However, no temperature measurements were performed. The experimental uncertainty for the measured quantities was in the order of 20% and 30% for the mean and turbulent statistics, respectively. It is worth noting that the reported experimental uncertainty is relatively high in this case. Fire experiments, as opposed to combustion experiments, typically involve much larger domains (making e.g. ambient conditions to be less well-controlled), are of larger scale (e.g. larger diameters of fuel inlet), often have less well-defined fuel source conditions (e.g. turbulence intensity), the presence of radiation and soot generation can be significant (e.g. particularly for hydrocarbon fuels) and difficulties in the exact measuring of certain quantities are present (e.g. surface or in-depth temperatures in case of flame spread, etc). All these factors combined contribute in typically having bigger experimental uncertainties when it comes to fire experiments as opposed to combustion experiments. One of the the main reasons for considering this test case in our work is the fact that it is part of the MaCFP Working Group (http://www.iafss.org/macfp/) which emphasizes on making systematic progress in fire modelling based on fundamental understanding of fire phenomena [14,15]. In the absence of a better large-scale test case with smaller experimental uncertainties these experiments were deemed sufficient for consideration by the authors. An overview of the initial and boundary conditions of the different experimental tests considered in this study is presented in Table 1.

This set of large-scale fire plume tests performed by Tieszen et al. [12,13] has provided an experimental database useful for validation of CFD codes. Several numerical studies using different modeling approaches have appeared in literature in the past focusing on these particular experiments. Ferraris et al. [16] performed large eddy simulations in order to investigate the possibility of employing the Conditional Source Estimation (CSE) as a model of low computational cost for large

Table 1 Initial and boundary conditions of the experiments [12,13].

Test	Fuel	D (m)	$\dot{m}''_{fuel}$ (kg/s)	$\dot{Q}_c$ (MW)	T_{fuel} (K)	T_∞ (K)	P_∞ (kPa)
#14	CH_4	1.0	0.040	1.59	284	285	80.6
#24	CH_4	1.0	0.053	2.07	286	290	81.0
#17	CH_4	1.0	0.066	2.61	274	278	81.1

fire simulations. Black et al. [17] performed RANS simulations with two different turbulence treatments, a steady RANS solution with a model for buoyancy-generated turbulence, and an unsteady solution with closure models based on a temporal filter width. DesJardin et al. [18] used LES to apply flamelet modeling combined with an alternative closure for the conditional dissipation rate, based on a transport equation for the mixture fraction filtered probability density function. Xin et al. [19] performed LES in order to validate an earlier version of the Fire Dynamics Simulator (FDS) while Pasdarshahri et al. [20] applied LES with OpenFOAM using the one-equation turbulence model. Hu et al. [21], also within the LES context, used detailed chemistry based on the the laminar flamelet approach and investigated the influence of chemical kinetics on the vortical structures of large-scale fires. Finally, these large-scale fire plume experiments have also been considered by the FDS developers for validation purposes of their code with numerical results reported in the software's validation guide [22].

3 Governing equations

FireFOAM, developed by FM Global, is a C++, object-oriented, LES code based on OpenFOAM. It is a second order accurate, finite volume code with implicit time integration and unstructured mesh capabilities [23]. FDS, developed by NIST, is a low-Mach number, LES code written in Fortran. It is a second order accurate, finite difference code with explicit time marching that uses structured grids. Given the fact that both FireFOAM and FDS are very comprehensive codes, all the technical details related to the numerical methods and solution algorithms employed in each CFD package cannot be presented here. The reader is directed to [24,25] for more details on FireFOAM and in [26] for FDS. Both codes solve conservation equations for mass, momentum, chemical species and sensible enthalpy using Favre-filtered quantities (e.g. $\widetilde{\phi} = \overline{\rho\phi}/\overline{\rho}$):

$$\frac{\partial \overline{\rho}}{\partial t} + \nabla \cdot (\overline{\rho}\widetilde{u}) = 0 \tag{1}$$

$$\frac{\partial (\overline{\rho}\widetilde{u})}{\partial t} + \nabla \cdot (\overline{\rho}\widetilde{u}\widetilde{u}) = -\nabla \overline{p} + \nabla \cdot \left[\mu_{eff}\left(\nabla \widetilde{u} + (\nabla \widetilde{u})^T - \frac{2}{3}(\nabla \cdot \widetilde{u})I\right)\right] + \overline{\rho} g \tag{2}$$

$$\frac{\partial (\overline{\rho}\widetilde{Y}_k)}{\partial t} + \nabla \cdot (\overline{\rho}\widetilde{u}\widetilde{Y}_k) = \nabla \cdot \left[\overline{\rho}\left(D_k + \frac{\nu_{sgs}}{Sc_t}\right)\nabla \widetilde{Y}_k\right] + \overline{\dot{\omega}'''_k}, \quad (k = 1, ..., N_s - 1) \tag{3}$$

$$\frac{\partial (\overline{\rho}\widetilde{h}_s)}{\partial t} + \nabla \cdot (\overline{\rho}\widetilde{u}\widetilde{h}_s) = \frac{\overline{Dp}}{Dt} + \nabla \cdot \left[\overline{\rho}\left(D_{th} + \frac{\nu_{sgs}}{Pr_t}\right)\nabla \widetilde{h}_s\right] - \nabla \cdot \overline{\dot{q}''_r} + \overline{\dot{q}'''_c} \tag{4}$$

where $\overline{\rho}$ is the density, $\widetilde{u}$ is the velocity, $\overline{p}$ is the pressure, $\mu_{eff} = \mu + \mu_{sgs}$ is the effective dynamic viscosity, μ is the laminar viscosity, $\mu_{sgs} = \overline{\rho}\nu_{sgs}$ is the sub-grid

scale viscosity, I is the identity tensor, g is the gravitational acceleration, $\widetilde{Y}_k$ is the species mass fraction, D_k is the species mass diffusivity, Sc_t is the turbulent Schmidt number, $\overline{\dot{\omega}_k'''}$ is the species reaction rate, $\widetilde{h}_s$ is the sensible energy, D_{th} is the thermal diffusivity, Pr_t is the turbulent Prandtl number, $\overline{\dot{q}_r''}$ is the radiative heat flux, $\overline{\dot{q}_c'''} = \Delta H_c \overline{\dot{\omega}_F'''}$ is the heat release rate per unit volume due to combustion (assuming complete combustion, i.e. $\chi = 1$) and ΔH_c is the heat of combustion of the fuel.

Both codes have a variety of turbulence and combustion models available for use. In the current study, the well-known constant coefficient Smagorinsky model [27] is used to model turbulence in FireFOAM (since there is no dynamic formulation of the model available yet) while its extension, the dynamic Smagorinsky, proposed by Lilly [28] with the model constant calculated by a dynamic procedure, is used in FDS. The sub-grid scale dynamic viscosity is then calculated as:

$$\mu_{sgs} = \overline{\rho}(c_s \Delta)^2 |\widetilde{S}| \tag{5}$$

where c_s is a model parameter, Δ is the LES filter size (e.g. cubic root of the cell volume) and $\widetilde{S} = \frac{1}{2}\left(\nabla \widetilde{u} + \nabla \widetilde{u}^T\right)$ is the strain rate tensor. In FireFOAM, the model parameter c_s is assigned a constant positive value while in FDS it can vary locally in both time and space. For stability reasons in FDS, negative c_s values are clipped to zero ($c_s \geq 0$), hence, back-scattering effects are not considered (energy transfer from the small to the large scales). For the dynamic implementation of the Smagorinsky model, a test filter of twice the grid size is employed in FDS. As part of a sensitivity study, the modified Deardorff model [29] is also applied in the numerical simulations with FDS since it is the standard turbulence model of the code. Within this model, the sub-grid scale dynamic viscosity is calculated as:

$$\mu_{sgs} = \overline{\rho} c_v \Delta \sqrt{k_{sgs}} \tag{6}$$

where $c_v = 0.1$ [30] is a model constant and k_{sgs} is the sub-grid scale kinetic energy. The sub-grid scale kinetic energy is calculated by the same model (the only available option in the software) in both the dynamic Smagorinsky and the modified Deardorff turbulence models in FDS (see Eq. (10) presented below). Unless stated otherwise, results with the dynamic Smagorinsky are presented by default in the paper. Some results with the modified Deardorff model are also presented in the paper for comparative purposes only.

The combustion model applied in both codes employs a one-step, infinitely fast, irreversible chemical reaction for CH_4:

$$CH_4 + 2(O_2 + 3.76N_2) \rightarrow CO_2 + 2H_2O + 7.52N_2 \tag{7}$$

combined with a modified Eddy Dissipation Model (EDM) model [31] to deal with turbulence-chemistry interactions. Within the EDM model the fuel mass reaction rate is calculated as:

$$\overline{\dot{\omega}_F'''} = \overline{\rho} \frac{min(\widetilde{Y}_F, \widetilde{Y}_{O_2}/s)}{\tau_{mix}} \tag{8}$$

where $\widetilde{Y}_F$ and $\widetilde{Y}_{O_2}$ are the fuel and oxygen mass fractions, respectively and s is the stoichiometric oxygen-to-fuel mass ratio. The $\overline{\dot{\omega}_k'''}$ for the others species are obtained through simple stoichiometric relations. The simplified consideration of

infinitely fast chemistry is a typical assumption made in CFD codes for fire simulations given the fact that, in most cases, it is the prediction of temperature and main species concentrations that are of relevance in fire safety and not so much the intermediate species, which would require the use of detailed chemistry. Within this framework, no chemical kinetics effects are considered within the combustion model, rather, chemistry is simplified into the calculation of mixing time scales under different conditions between the fuel and oxidizer. The main difference between the combustion model in the two codes lies in the calculation of the mixing time scale, τ_{mix}. In FireFOAM, the turbulent (k_{sgs}/ϵ_{sgs}) and molecular (Δ^2/α) diffusion time scales are considered when calculating the fuel mass reaction rate, proving this way an estimate of the fuel-air mixing, under turbulent and laminar flow conditions, respectively. On the other hand, a more detailed reaction time scale model is used in FDS in which the chemical time scale is compared with the mixing times for diffusion (Δ/D_F, where D_F is the fuel mass diffusivity), sub-grid scale advection ($\Delta/\sqrt{2k_{sgs}}$) and buoyant acceleration ($\sqrt{(2\Delta/g)}$ [32]. This reaction time scale model proposes a scaling regime for coarse mesh resolution based on buoyant acceleration. As explained in [32], for fires which are generally buoyancy-driven flows, buoyant acceleration is expected to control the mixing at relatively coarse scales. Hence, a time scale based on a constant acceleration that scales with the square root of the filter width is proposed. Both τ_{chem} and τ_{flame} are effectively not used in the current simulations but pose the extreme limits that τ_{mix} can take in the reaction time scale model.

The estimation of the sub-grid scale kinetic energy, k_{sgs}, needed for calculating the mixing scale scale, τ_{mix}, in the EDM combustion model is done differently in the two codes. In FireFOAM, different ways of calculating k_{sgs} exist depending on the applied turbulence model. Within the Smagorinsky model, the assumption of local equilibrium is used and k_{sgs} is obtained from a balance equation as:

$$\overline{\rho}(\widetilde{S} : B) + \frac{c_e \overline{\rho} k_{sgs}^{3/2}}{\Delta} = 0 \tag{9}$$

where ':' denotes the double inner product, $B = \frac{2}{3}k_{sgs}I - 2c_k\sqrt{k_{sgs}}\Delta\ \widetilde{S}_D$ is the sub-grid stress tensor, $\widetilde{S}_D$ is the deviatoric component of the strain rate tensor, and $c_k = 0.05$, $c_e = 1.048$ [33] are two model constants. The sub-grid scale dissipation rate, ϵ_{sgs}, is then approximated as $\epsilon_{sgs} = c_e k_{sgs}^{3/2}\Delta^{-1}$. On the other hand, in FDS k_{sgs} is approximated based on scale similarity arguments as:

$$k_{sgs} = \frac{1}{2}\left[(\overline{u} - \hat{u})^2 + (\overline{v} - \hat{v})^2 + (\overline{w} - \hat{w})^2\right] \tag{10}$$

where $\overline{u}$, $\overline{v}$, $\overline{w}$ are the average values of u, v, w in the cell centers and $\hat{u}$, $\hat{v}$, $\hat{w}$ are the weighted averages of u, v, w in the adjacent cells.

A commonly used radiation model is adopted in this study in which the radiative intensity is treated as a function of both spatial location and angular direction and is obtained by solving the radiative transfer equation (RTE) by the finite volume discrete ordinates model (fvDOM) accounting for attenuation and augmentation of radiation by absorption and emission, respectively:

$$\frac{\partial \widetilde{I}}{\partial s} = \widetilde{\kappa}\widetilde{I}_b - \widetilde{\kappa}\widetilde{I} \tag{11}$$

where I is the radiation intensity, s is the solid angle, I_b is the black body radiation intensity and κ is the absorption coefficient. Under the assumption of a grey gas ($\kappa_P = \kappa$) and considering an optically thin flame, neglecting scattering, the radiative heat flux is then calculated as:

$$\nabla \cdot \overline{\dot{q}_r''} = \widetilde{\kappa}_P \left(4\pi \widetilde{I}_b - \int_{4\pi} \widetilde{I} d\Omega \right) = \widetilde{\kappa}_p (4\sigma \widetilde{T}^4 - \widetilde{G}) \tag{12}$$

where κ_P is the mean Planck absorption coefficient, σ is the Stefan-Boltzmann constant, T is the (filtered) temperature and G is the total irradiance. The mean Planck absorption coefficients for the chemical species are temperature-dependent and calculated by the RADCAL model [34]. It is worth mentioning that contributions from turbulence-chemistry interaction (TRI) are neglected in Eq. (12). However, in FDS the source term of the RTE in the flame region is calculated as:

$$\nabla \cdot \overline{\dot{q}_r''} = \widetilde{\kappa}_p (4\sigma C \widetilde{T}^4 - \widetilde{G}) \tag{13}$$

where C is a constant, computed at each time step, which corrects the emission term in order to compensate for both errors in emissivity calculations and in TRI. A radiative fraction of $\chi_r = 0.2$ [35] is used in the present study, which represents the global fraction (lower limit) of energy that is released from combustion as thermal radiation.

No soot model was employed in either code since soot generation during CH_4 combustion is not significant [36]. The selected models for the numerical simulation with FireFOAM and FDS are outlined in Table 2 and Table 3, respectively.

Table 2 Models used in the FireFOAM simulations.

	FireFOAM 2.2.x
Turbulence model	Constant Smagorinsky $\mu_{sgs} = \overline{\rho}(c_s \Delta)^2 \lvert \widetilde{S} \rvert$ $c_s = 0.1$ [8]
Combustion model	Eddy Dissipation Model (EDM) $\overline{\dot{\omega}_F'''} = \overline{\rho} \frac{min(\widetilde{Y}_F, \widetilde{Y}_{O_2}/s)}{\tau_{mix}}$ $\tau_{mix} = min\Big(\underbrace{\frac{k_{sgs}}{C_{EDM} \epsilon_{sgs}}}_{\tau_{turb}}, \underbrace{\frac{\Delta^2}{C_{diff} \alpha}}_{\tau_{lam}} \Big)$ $C_{EDM} = 4$, $C_{diff} = 2$ [25]
Radiation model	Radiative Transfer Equation (RTE) Finite Volume Discrete Ordinates Method (FVDOM) 48 solid angles $\overline{\dot{q}_r''} = \kappa_p \big(4\sigma T^4 - G \big)$
Soot model	-

4 Numerical set-up

The computational domain employed in the numerical simulations is 4 m × 6 m of cylindrical shape for FireFOAM (Figure 1(a)) and 4 m × 6 m × 4 of rectangular

Table 3 Models used in the FDS simulations.

	FDS 6.1.2
Turbulence model	Dynamic Smagorinsky $\mu_{sgs} = \overline{\rho}(c_s \Delta)^2 \lvert\widetilde{S}\rvert$ c_s: determined dynamically
Combustion model	Eddy Dissipation Model (EDM) $\overline{\dot{\omega}_F^{'''}} = \overline{\rho}\frac{min(\widetilde{Y}_F, \widetilde{Y}_{O_2}/s)}{\tau_{mix}}$ $\tau_{mix} = max[\tau_{chem}, min(\tau_d, \tau_u, \tau_g, \tau_{flame})]$ $\tau_d = \frac{\Delta^2}{D_F}$, $\tau_u = \frac{\Delta^2}{\sqrt{(2k_{sgs})}}$, $\tau_g = \sqrt{\frac{2\Delta}{g}}$
Radiation model	Radiative Transfer Equation (RTE) Finite Volume Discrete Ordinates Method (FVDOM) 100 solid angles $\overline{\dot{q}_r^{''}} = \kappa_p\big(4\sigma C T^4 - G\big)$: Inside flame zone $\dot{q}_r^{''} = \kappa_p\big(4\sigma T^4 - G\big)$: Outside flame zone C: correction factor
Soot model	-

shape for FDS (Figure 1(b)). The 1 m in diameter fire source is modeled by specifying the corresponding mass flow rate reported in the experiments. The surrounding 0.51 m wide steel floor (ground plane) was modeled as adiabatic. The bottom plane ($y = 0\ m$), outside the steel floor, along with the sides and the outlet of the computational domain were set as open, allowing air to be entrained into the domain. The mesh was refined around the centerline (half an inlet diameter outside the fire source and up to the outlet) which resulted in grid sizes of $\approx$ 1.5 cm in the areas of interest and 66 cells across the fire source. The grid spacing used outside the refined region was 3 cm for FDS and varied from 3 cm (just outside the refined region) to 6 cm (sides of the domain) in FireFOAM. The total number of cells was then $\approx$2.38 million for FireFOAM and $\approx$8.65 million for FDS. It is exactly this different meshing technique employed in the numerical simulations that results in the difference in the total number of cells used with the two software. Nevertheless, this is of secondary importance since approximately the same cell size ($\approx$ 1.5 cm around the centerline) is used in the main area of interest (above the fuel inlet and on the centerline). All numerical simulations were set to run for 50 sec with a varying time step, limited by a maximum Courant number of 0.8. Averaging was employed during the last 45 sec of the numerical simulations. In FireFOAM, the equations are advanced in time using a second order implicit Euler scheme. All quantities are assigned to the cell centers (collocated grid) with velocities linearly interpolated to the cell faces. The convective terms are second order centrally differenced. For scalar transport, a second order TVD scheme using a Sweby limiter is applied while the diffusive terms are centrally differenced and corrected for the non-orthogonality of the mesh. A PISO algorithm is used for the pressure-velocity coupling with a Rhie-Chow interpolation to avoid odd-even decoupling. The pressure equation is solved by a linear GAMG solver. In FDS, the governing equations are advanced in time by using a second order explicit Runge-Kutta scheme. Spatial derivatives are estimated with second-order finite differences on a rectangular grid, with scalar quantities assigned to the cell center and velocities assigned to the cell faces. Convective terms are upwind biased,

based on a Courant-Friedrichs-Lewy condition, in the predictor step and downwind biased in the corrector step. If the Courant number is near unity, this corresponds to a nearly fully upwind scheme, while for a Courant number much less than unity, the scheme is more centralized. This second-order finite differencing scheme of FDS cannot, however, fully resolve sharp gradients on a relatively coarse grid. Steep gradients can cause local over-shoots and under-shoots in quantities like density and species mass fraction. For this reason, a flux correction scheme is performed in both the predictor and corrector steps to ensure that the quantities stay bounded. The second-order TVD scheme, SuperBee, is used for scalar transport and the diffusive terms are central differenced. A fast Fourier transform based solver solves the Poisson equation. The turbulent Schmidt and Prandtl numbers were set to 0.7. The initial and boundary conditions used in the numerical simulations were set according to the experiments, previously reported in Table 1. For the numerical simulations with both codes, the corresponding mass flow rate and a fixed value for temperature was applied at the inlet. In FireFOAM, a mixed boundary condition is assigned for velocity at the sides of the domain, setting zero gradient for any outward flow and calculating the inlet velocity from pressure. A Dirichlet boundary condition is assigned for pressure at the sides of the domain, which fixes total pressure and when velocity changes, the pressure is adjusted accordingly. In FDS, all boundaries of the computational domains were considered as 'open' (natural ventilation) allowing for flow into or out of the computational domain depending on the local pressure gradient. An overview of the numerical set-up used for the numerical simulations with the two codes is presented in Table 4.

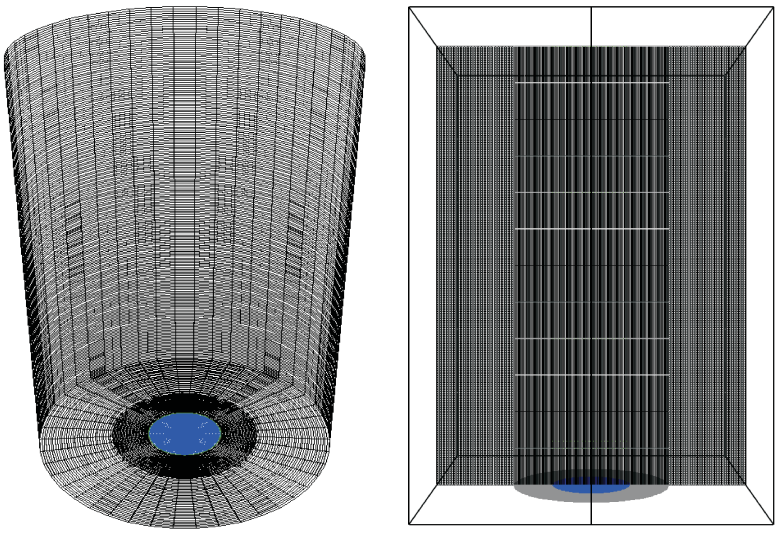

(a) (b)

Fig. 1 Computational mesh used in the simulations with (a) FireFOAM and (b) FDS.

Table 4 Numerical set-up used in the simulations.

	FireFOAM 2.2.x	**FDS 6.1.2**
Domain	4 m × 6 m (cylindrical)	4 m × 6 m × 4 m (rectangular)
Number of cells	≈ 2.38 million	≈ 8.65 million
Grid type	Non-uniform	Non-uniform
Grid size (centerline)	≈ 1.5 cm	1.5 cm
Cells across inlet	66	66
Run time	50 sec (45 sec averaging)	50 sec (45 sec averaging)
Time step	Varying (max $Co = 0.8$)	Varying (max $Co = 0.8$)

5 Results

5.1 Instability generation

A key element for accurately predicting the instability generation at the base of the source and the resulting puffing frequencies of buoyant helium and fire plumes is having good mesh resolution in the near-field region of the plumes. In both cases there are vastly different scales involved: the small scales, related to mixing, and the large scales, related to the characteristic puffing motion. For all the test cases considered in this study, the conditions at the source were laminar (inlet velocities of only a few cm/s), but very quickly buoyancy-generated turbulence makes the flow turbulent (within an inlet diameter distance). The triggering mechanism [8,9,18] is the generation of instabilities at the edges of the source due to baroclinic and gravitational torques. If coarse grids are used in the numerical simulations then small-scale mixing is not well captured and temperatures are typically under-predicted, resulting in smaller density gradients. As a consequence, such instabilities are significantly smoothened out at the base of the source, resulting in no clear puffing frequency. It was found that grid sizes of 1.5 cm are sufficiently small to accurately predict the instability generation at the base of the source and to obtain a correct puffing frequency. This grid size can be expressed in a dimensionless way if we define a Plume Resolution Index (PRI) [22], expressing the number of grid cells of length Δx (m) that span the characteristic diameter of the fire, D^* (m), defined as:

$$PRI = \frac{D^*}{\Delta x} \tag{14}$$

with the characteristic fire diameter expressed as [37]:

$$D^* = \left(\frac{\dot{Q}}{\rho_\infty c_p T_\infty \sqrt{g}} \right)^{2/5} \tag{15}$$

where $\dot{Q}$ (kW) is the heat release rate, ρ_∞ (kg/m^3) is the ambient density, c_p (kJ/kg·K) is the heat capacity, T_∞ (K) is the ambient temperature, g (m/s^2) is the gravitational acceleration while Δx (m) is the width of the grid cells at the

fire source. The higher the PRI values the more 'resolved' is the fire dynamics in the numerical simulations. Nevertheless, PRI should only be used as an indicator of the quality of the mesh of a given numerical study and it is not intended as a replacement of a grid sensitivity study. Such a grid sensitivity study is presented at the end of the paper for completeness. In literature, PRI values ranging between 5-15 have proven to give satisfactory accuracy with an acceptable computational time for many fire scenarios [22], values up to 16 were used when simulating fire plume scenarios [38] while values up to 40 were reported to be sufficient for a 1-m in diameter turbulent buoyant helium plume [39]. In the present study, the PRI values were approximately between 84 (for Test #14)-102 (Test #17) which are sufficiently large enough to adequately capture the flow evolution and unsteady behavior of these fire plumes. Similar PRI values have also been used by the FDS developers in their validation study of the same test case [22].

The puffing cycle of a fire plume, shown in Figure 2, is similar to the one of a buoyant plume and can be broken down into four distinct stages: the generation of the instability near the edge of the source due to baroclinic and gravitational torques (Figure 2(a)), the growth of the instability towards the center of the source (Figure 2(b)), the triggering of the Rayleigh-Taylor instability which generates large toroidal vortices (Figure 2(c)) and the convection of these vortices downstream until they break down due to generated secondary instabilities and Kelvin-Helmholtz instabilities (Figure 2(d)). These stages are then repeated in every puffing cycle [8,9,18]. The low inlet velocity and the strong deflection of the plume from the axial direction at the source edges, indicate that vorticity from the source is not responsible for the formation of turbulent structures at the plume-air interface. Rather, they are formed by buoyancy-driven vorticity generation [8].

The vorticity generation mechanism in fire plumes differs from previously studied iso-thermal buoyant plumes [8,9]. In the latter, there is a monotonic decrease of density with increasing radius from the center of the source and the generated vorticity is limited to the base of the source (near the two-fluid interface) where the density gradients are maximum. In the former, density initially decreases with increasing radius from the centerline until the reaction zone where it starts increasing again moving towards the air side, resulting in a more localized vorticity distribution. This effect generates a set of counter-rotating vortices on either side of the flame zone, causing fuel and oxidizer to be brought into the reaction zone [18]. This is illustrated in Figure 3, where the baroclinic and gravitational torques with FireFOAM for Test #17 are presented at different heights. The baroclinic torque is generated due to misaligned density and pressure gradients while the gravitational torque due to misaligned density gradients and gravity. Both the baroclinic and gravitational torques are responsible for the instability generation at the base of the source (Figure 3(a)), however, only the influence of the baroclinic torque remains significant with increasing height from the fire source (Figure 3(c)). The same observations were also made in the study of a turbulent, buoyant helium plume of the same source size [8]. At height $y = 0.5\ m$ (0.5D) the magnitude of the inner baroclinic torque (at locations $r = \pm 0.05\ m$) exhibits about half the magnitude of the outer baroclinic torque (at locations $r = \pm 0.15\ m$) since the density gradients from the center of the fire source to the reaction zone are significantly smaller than the density gradients from the reaction zone to the surrounding air (Figure 3(b)). However, on the centerline and up to the location of the maximum flame temperature, density is decreasing with increasing height so that the den-

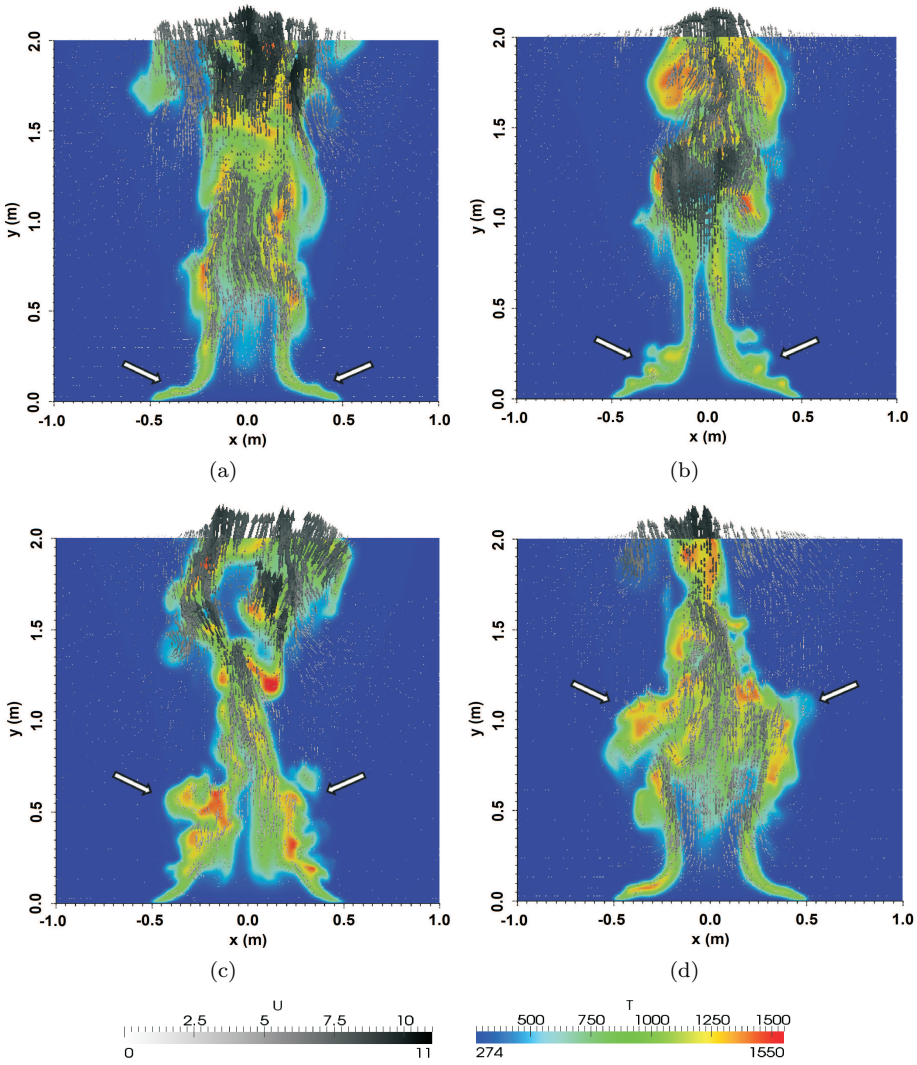

Fig. 2 Puffing cycle with FireFOAM for Test #17 at time (a) 30.0 s, (b) 30.2 s, (c) 30.4 s and (d) 30.6 s.

sity gradients also become smaller, thus decreasing the magnitude of the inner baroclinic torque ((Figure 3(c))).

5.2 Mean and rms quantities

According to Pope's criterion [40], a turbulence resolution of more than 80% is needed for accurate LES. Nevertheless, this criterion should be used cautiously since depending on how the sub-grid scale kinetic energy, k_{sgs}, is calculated, numerical dissipation introduced by the numerical schemes used for discretization is

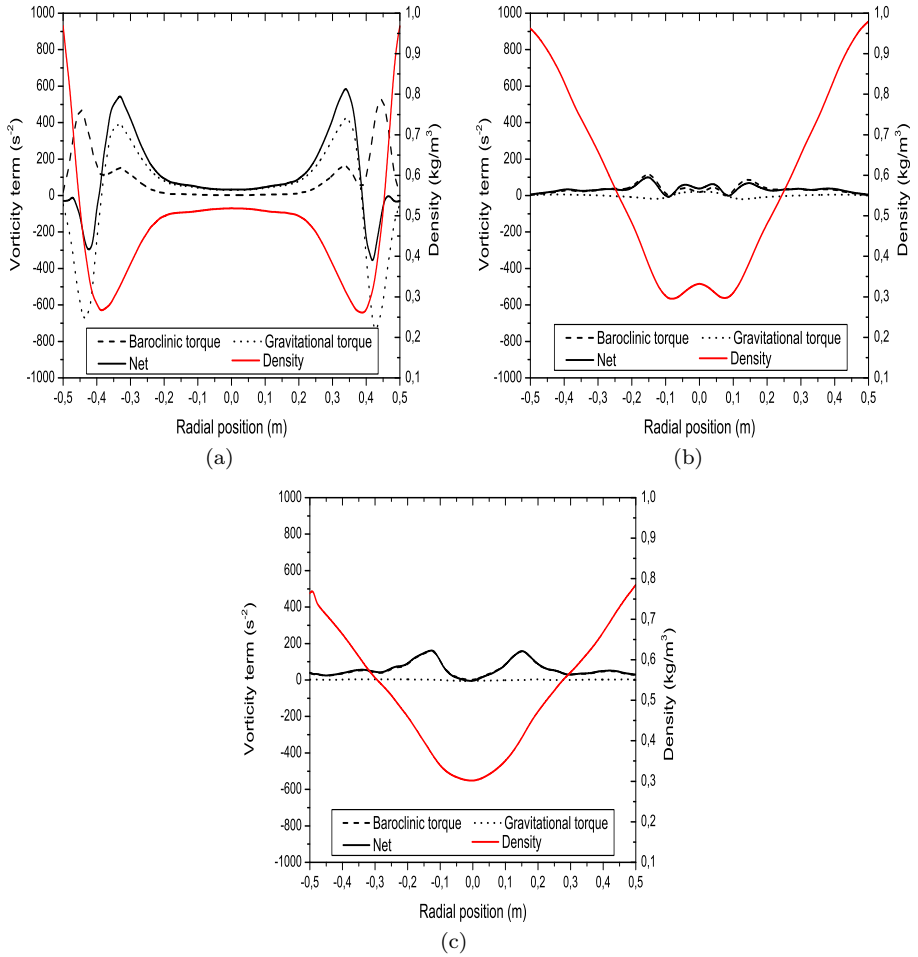

Fig. 3 Baroclinic and gravitational torques with FireFOAM for Test #17 at height (a) $y = 0.05\ m$, (b) $y = 0.5\ m$ and (c) $y = 1.5\ m$.

not explicitly accounted for in the calculation of the turbulence resolution. This type of criterion tends to lead to an over-estimation of the simulation quality if the amount of numerical dissipation is increased, i.e. when the quality of the simulation is actually lowered by using too dissipative schemes [41]. The turbulent resolution in all numerical simulations (not shown here) remained above Pope's suggested value, however, the real value is likely lower due to the reasons mentioned above and due to the tendency of the sub-grid scale models to being "optimistic" in the calculation of k_{sgs}.

Simulation results of the mean and rms quantities as function of radial positions at different heights, y, and on the centerline are presented in this section. The symbols depict experimental data and predictions of experimental correlations while the grey areas represent the experimental uncertainty of the measurements. Focusing on the plume region (Table 5) of fire plumes, Heskestad's experimental

correlations [42] give an estimate of the centerline axial velocities:

$$v = 3.4\left(\frac{g}{c_p T_\infty \rho_\infty}\right)^{1/3} \dot{Q}_c^{1/3}(y-y_0)^{-1/3} \tag{16}$$

and centerline temperatures:

$$T = 9.1\left(\frac{T_\infty}{g c_p^2 \rho_\infty^2}\right)^{1/3} \dot{Q}_c^{2/3}(y-y_0)^{-5/3} + T_\infty \tag{17}$$

where T_∞, c_p and ρ_∞ are the temperature, heat capacity and density of ambient air, respectively, and $\dot{Q}_c = \chi_r \dot{Q}$ is the convective heat release rate, with a radiative fraction of $\chi_r = 0.2$, as reported from the experimental study by Hamins et al.[35]. The virtual origin of the plume, y_0, depends on the diameter of the fire source, D, and the total heat release rate, $\dot{Q}$, and according to Heskestad's correlation [42] it can be estimated as:

$$y_0 = 0.083\dot{Q}^{2/5} - 1.02D \tag{18}$$

Table 5 Summary of the different regions in the fire plumes [3].

Test	Flame region $\left(\frac{y}{\dot{Q}^{2/5}} < 0.08\right)$	Intermittent region $\left(0.08 < \frac{y}{\dot{Q}^{2/5}} < 0.2\right)$	Plume region $\left(\frac{y}{\dot{Q}^{2/5}} > 0.2\right)$
#14	$y < 1.52\ m$	$1.52 < y < 3.81\ m$	$y > 3.81\ m$
#24	$y < 1.69\ m$	$1.69 < y < 4.24\ m$	$y > 4.24\ m$
#17	$y < 1.86\ m$	$1.86 < y < 4.65\ m$	$y > 4.65\ m$

McCaffrey's experimental correlations [3] can also be used to get an estimate of the centerline axial velocities and temperatures in the plume region:

$$v = 1.1\left(\frac{y}{\dot{Q}^{2/5}}\right)^{-\frac{1}{3}} \dot{Q}^{1/5} \tag{19}$$

$$T = T_\infty \left(\frac{1.1}{0.9(2g)^{1/2}}\right)^2 \left(\frac{y}{\dot{Q}^{2/5}}\right)^{-\frac{5}{3}} + T_\infty \tag{20}$$

5.2.1 Velocities

The predicted axial and radial velocities with FireFOAM and FDS at different heights, y, are presented in Figures 4-9 for the test cases considered. It is observed that axial velocities increase with higher elevations due to the flow acceleration induced by strong buoyancy forces on the plume axis. With increasing distance from the fire source, the velocity profiles also become wider due to the fire plume spreading. On the contrary, the radial velocities obtain their maximum values close to the fire source due to strong air entrainment towards the plume axis generated by the vorticity generation mechanisms. The trends of the mean axial and radial velocity profiles in the near-field region ($y < 1.0\ m$) are well captured by both codes for all cases examined and in most cases remain within experimental uncertainty.

No significant differences are evident in the predicted results, revealing that both CFD codes can predict both qualitatively and quantitatively the mean flow field associated with large-scale fire plumes. Nevertheless, FDS maintains the 'double peak' in the velocity profile longer than FireFOAM. This can be explained by the higher temperatures obtained with FireFOAM (causing stronger acceleration) and by the less turbulence observed in FDS (leading to less mixing) on the centerline, presented later in the paper. Some discrepancies between the simulations and the experiments are present, e.g., in the axial velocities at height $y = 0.9\ m$ for Test #14 and in the radial velocities for the cases with higher heat release rate. However, the possibility of errors in the experimental measurements should not be excluded since, e.g., the reported velocities for Test #14 at height $y = 0.9\ m$ are lower than at height $y = 0.5\ m$ (Figure 4) which is not consistent with the velocity measurements of the rest of the tests.

The mean and rms centerline axial velocities are reported in Figure 10. The rapid transition of the flow from laminar to turbulent, created by strong buoyancy forces, is evident. Even though the inlet conditions in the experiments were laminar (inlet velocities of only a few cm/s), the axial velocities reach up to 5-6 m/s within 1 diameter. It is observed that the laminar to turbulent transition is well predicted by both codes and no significant differences are observed in the flame region. In general, the predicted axial velocities by both FireFOAM and FDS compare favorably with both the experimental results and the experimental correlations in the plume region for all the test cases. Some over-prediction of the axial velocities by FireFOAM in the plume region is, however, observed. Both codes predict the same level of axial velocity fluctuations in all regions of the fire plumes with no significant differences in the profiles.

By analyzing the axial evolution of the Smagorinsky constant in the FDS simulations (Figure 11) it is observed that the constant gradually increases with axial distance from the fire source until it reaches an almost constant value of $c_s \approx 0.13$ at locations $y/D > 3$. This constitutes a 30% increase of the constant in the FDS simulations with the dynamic Smagorinsky when compared to the constant value of $c_s = 0.1$ that was used in FireFOAM and can partially explain the small differences in the axial velocities observed between the two codes in the plume region. It is expected that if the model constant c_s in the Smagorinsky model in FireFOAM was determined dynamically, accounting for the local properties of the flow, it would predict more accurately the velocities in the intermittent and plume regions of these large-scale fire plumes.

5.2.2 Mixing time scales and reaction rates

Figure 12 presents the evolution of the centerline mixing time scales (τ_{mix}) and fuel reaction rates ($\overline{\dot{\omega}_F'''}$) for Test #17 (the results for the other two cases were in the same order of magnitude and are omitted to avoid repetition). In general, significant differences are observed between the two codes. Higher mixing times scales than FDS are evident with FireFOAM, very close to the inlet, at locations $y < 0.5\ m$. At heights $y > 2.0\ m$ the predicted mixing time scales with FireFOAM ($\tau_{mix} = 0.12\ s$) remain approximately two times lower than FDS ($\tau_{mix} = 0.056\ s$) at all axial locations examined. These lower τ_{mix} values in FireFOAM imply that mixing between fuel and oxidizer requires less time (i.e. is faster) in FireFOAM than in FDS, thus enhancing combustion and producing higher temperatures. It is

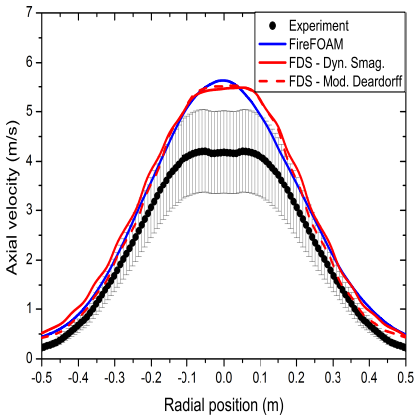

(a)

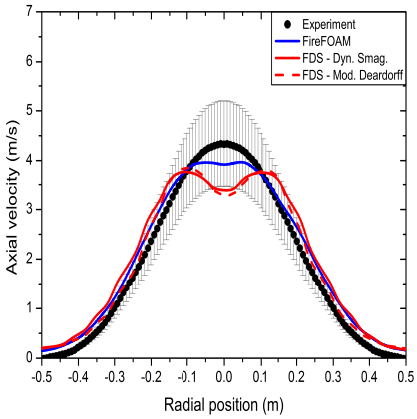

(b)

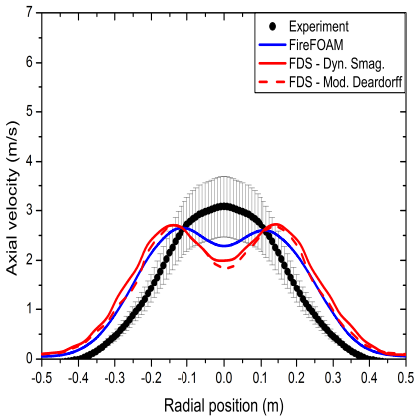

(c)

Fig. 4 Axial velocities for Test #14 at height (a) $y = 0.9\ m$, (b) $y = 0.5\ m$ and (c) $y = 0.3\ m$.

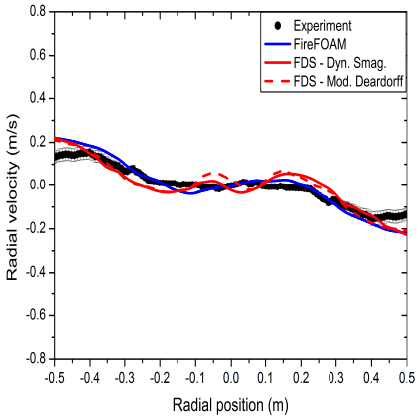

(a)

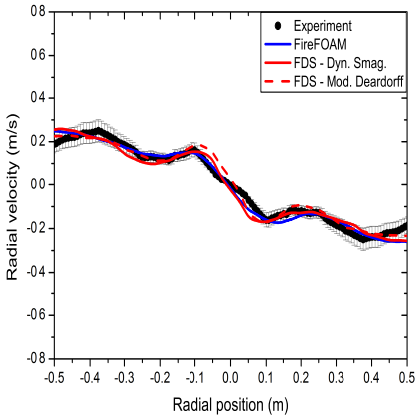

(b)

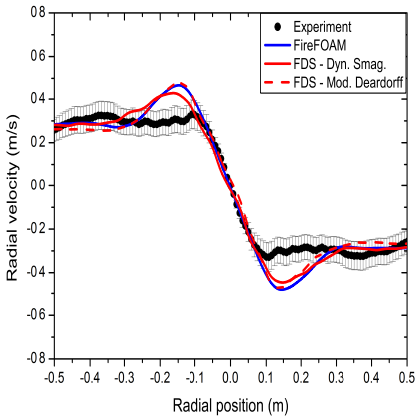

(c)

Fig. 5 Radial velocities for Test #14 at height (a) $y = 0.9\ m$, (b) $y = 0.5\ m$ and (c) $y = 0.3\ m$.

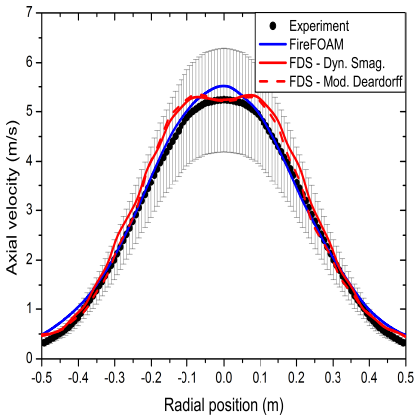

(a)

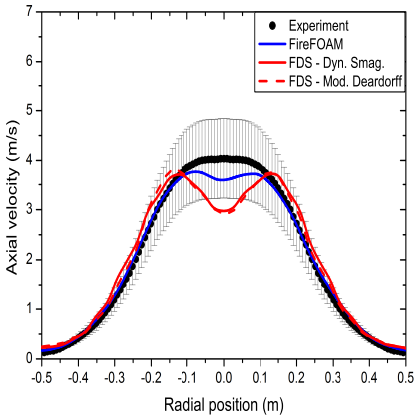

(b)

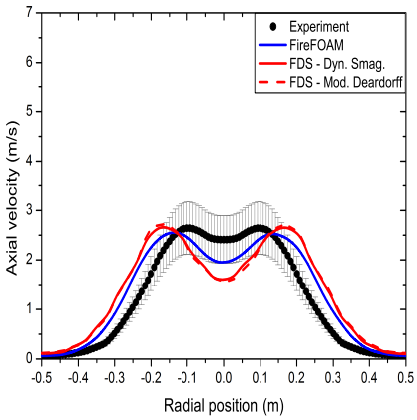

(c)

Fig. 6 Axial velocities for Test #24 at height (a) $y = 0.9\ m$, (b) $y = 0.5\ m$ and (c) $y = 0.3\ m$.

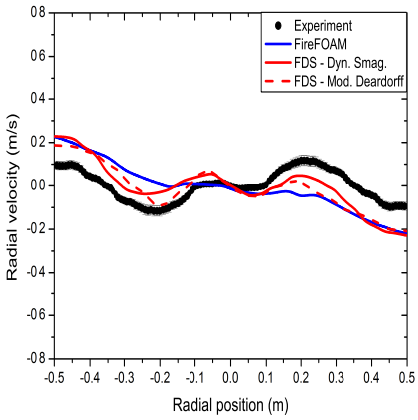

(a)

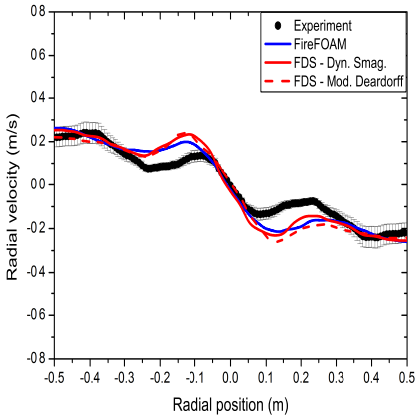

(b)

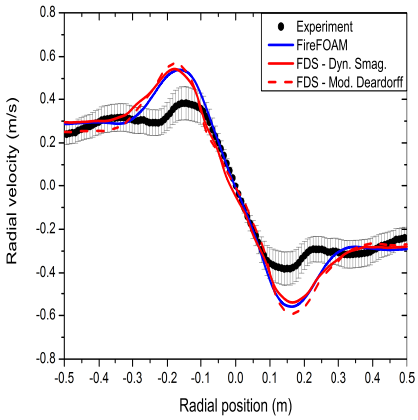

(c)

Fig. 7 Radial velocities for Test #24 at height (a) $y = 0.9\ m$, (b) $y = 0.5\ m$ and (c) $y = 0.3\ m$.

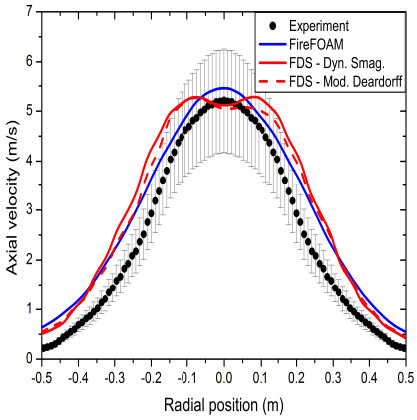

(a)

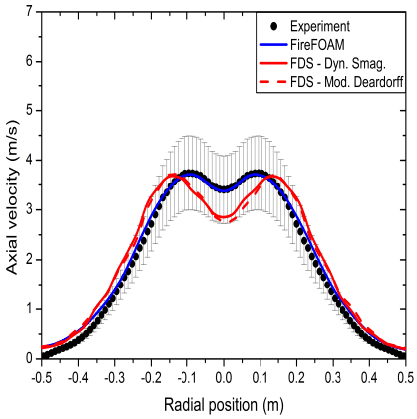

(b)

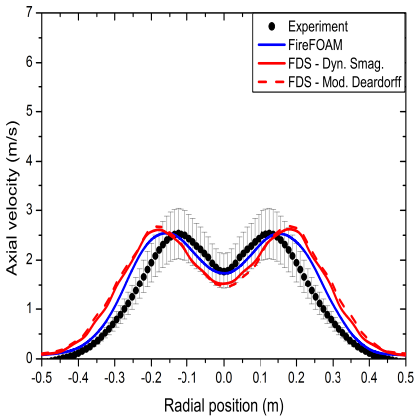

(c)

Fig. 8 Axial velocities for Test #17 at height (a) $y = 0.9\ m$, (b) $y = 0.5\ m$ and (c) $y = 0.3\ m$.

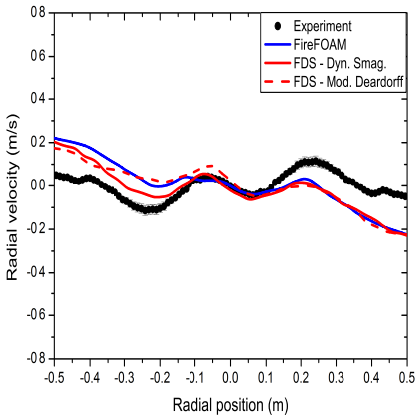

(a)

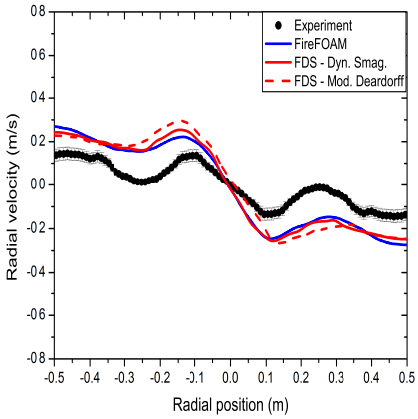

(b)

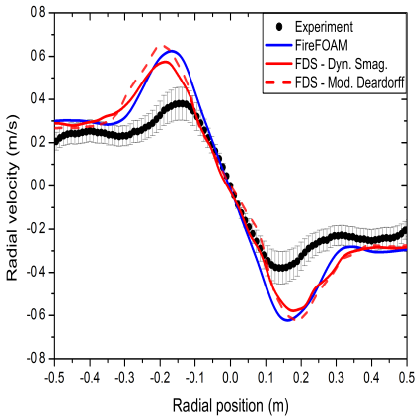

(c)

Fig. 9 Radial velocities for Test #17 at height (a) $y = 0.9\ m$, (b) $y = 0.5\ m$ and (c) $y = 0.3\ m$.

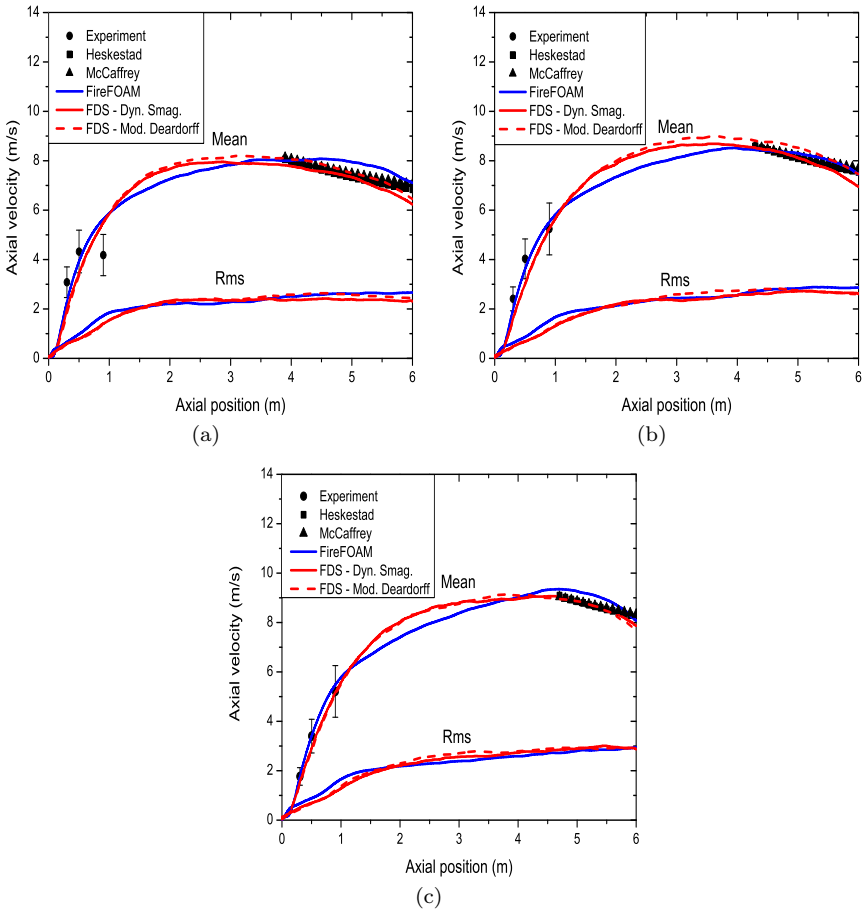

Fig. 10 Centerline axial velocities for (a) Test #14, (b) Test #24 and (c) Test #17.

worth noting that the predicted sub-grid scale kinetic energies, k_{sgs}, with the two codes at different heights and on the centerline (not shown here) were on the same order of magnitude, nevertheless, differences in the radial profiles up to a factor of two were evident. The differences that are observed in the mixing time scales are partially attributed to the fact that only turbulent and molecular mixing is accounted for in the version of the EDM combustion model used in FireFOAM, whereas, for the determination of τ_{mix} in FDS, the chemical mixing time scale is compared with the mixing times for diffusion, advection and buoyant acceleration. More specific, the different definition of τ_{turb} in FireFOAM and τ_u in FDS (or the different choice of constants in their derivation) leads to significant differences between these two time scales. The particular choice of constants here, $C_{EDM} = 4$ and $c_e = 1.048$, leads to $\tau_u \approx 2-3\tau_{turb}$ (depending also on the calculated values of k_{sgs}), which is clearly portrayed in Figure 12. More specifically, the mixing time scale due to molecular mixing in FireFOAM, τ_{lam} is, in this case, consistently higher than τ_{turb} and is not taken into account at all in the EDM model, rather

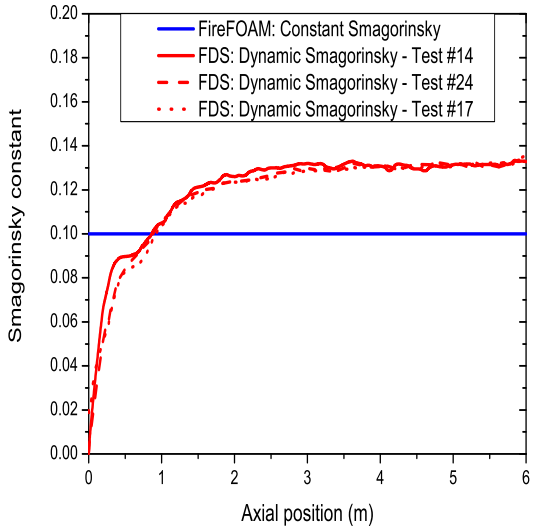

Fig. 11 Centerline evolution of the Smagorinsky constant, c_s.

only τ_{turb} is used. On the other hand in FDS, τ_g is important close to the fire source and τ_d becomes dominant further downstream. These differences in the mixing time scales between the two codes also contribute to the resulting fuel mass reaction rates where the peak $\overline{\dot{\omega}'''_F}$ values with FireFOAM are more than double than those of FDS. These high fuel reaction rates with FireFOAM in the flame region enhance combustion and produce hotter combustion products than FDS that are convected in the plume region, resulting in higher temperatures (shown below).

5.2.3 Temperatures

The predicted centerline temperatures with both codes are presented in Figure 13. In general, the predictions of FDS agree well with the experimental correlations in the plume region where over-predictions of up to 50 K are observed. This was expected since the axial velocity profiles were also well predicted. On the other hand, the centerline temperatures predicted by FireFOAM are over-predicted by up to 100 K in the plume region. This is a direct consequence of the previously reported slightly higher axial velocities compared to FDS (Figure 10) and higher reaction rates (Figure 12) convecting hotter combustion products into the plume region. Additionally, small differences are evident in the profiles of the temperature fluctuations at almost all axial locations examined, with FDS having higher fluctuations than FireFOAM.

5.2.4 Turbulent kinetic energies

Results of the turbulent kinetic energies (sum of resolved and modeled) are presented in Figure 14 for Test #24. The simulation results with FireFOAM agree well with the experimental values and remain close to the experimental uncertainty,

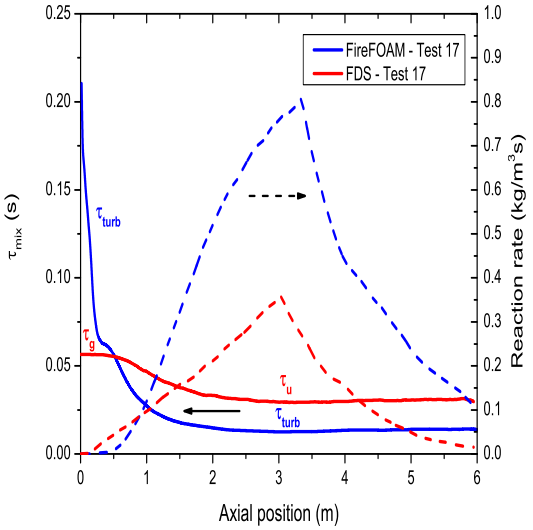

Fig. 12 Centerline evolution of the mixing time scales (τ_{mix}) and reaction rates ($\overline{\dot{\omega}_F'''}$) for Test #17.

revealing that the turbulent fluctuations in the near-field region of the fire plumes are well captured by the code. The turbulent kinetic energies predicted by FDS are less than FireFOAM, particularly around the centerline of the fire plumes, but remain in reasonable agreement with the experiments.

5.3 Puffing frequency

From experiments performed on pool fires of different source sizes and fuels it has been observed that the puffing frequency is strongly dependent on the fire source diameter and almost independent on the fuel type. Correlations for predicting the puffing frequencies of pool fires have been derived based on experiments performed by, e.g., Zukoski [43]:

$$f = 0.5\left(\frac{g}{D}\right)^{1/2} \; Hz \tag{21}$$

and Cetegen [44]:

$$f = 1.5\sqrt{D} \; Hz \tag{22}$$

The puffing frequency corresponds to the number of puffing cycles encountered, counted here as a maximum peak in the axial velocity followed by a minimum, in the given timeline examined. This puffing behavior is seen in Figure 15(a), presenting the time trace (6 sec) of the centerline axial velocity at height $y = 0.5\ m$ for Test #17. The time signals taken from the numerical simulations have been shifted along the time axis to make the comparison with the experiments more clear (i.e. inspection by eye to overall match the locations of the maxima observed in the experiments). A total of 10 cycles, corresponding to the passage of large-scale structures, are distinguished in the experimental data. In general, both codes are able to reproduce the puffing behavior of the CH_4 fire plume, also predicting

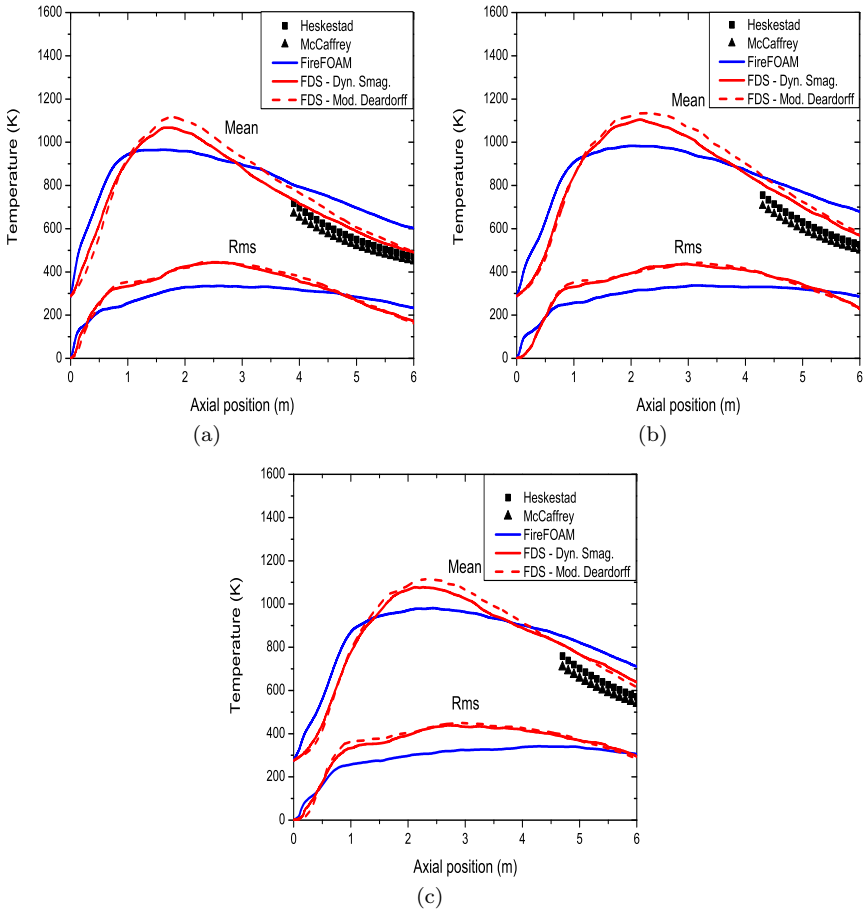

Fig. 13 Centerline temperatures for (a) Test #14, (b) Test #24 and (c) Test #17.

the same number of cycles in the same time period examined. Nevertheless, the amplitude of the axial velocity with FDS is smaller when compared to FireFOAM and the experimental data. However, if the time trace of temperature is considered at the same location ($y = 0.5\ m$) then a totally different behavior is observed between the two codes Figure 15(b). In this case, a puffing behavior is clearly observed only with FireFOAM while the temperature in the FDS simulations remains almost constant. This lack of temperature fluctuations in FDS was previously also seen in Figure 13.

Fast Fourier transformations of the time signals (taken between 5-50 sec in the numerical simulations) of the axial velocities and temperatures at height $y = 0.5\ m$ above the fire source were performed. The predicted amplitude spectrums are presented in Figures 16-17, respectively, and the resulting puffing frequencies presented in Tables 6-7, respectively. The smaller amplitude in the predicted centerline axial velocities with FDS, previously seen in Figure 15, is obviously confirmed. It is also observed that, for the same fuel, increasing the HRR from 1.59 (Test #14)

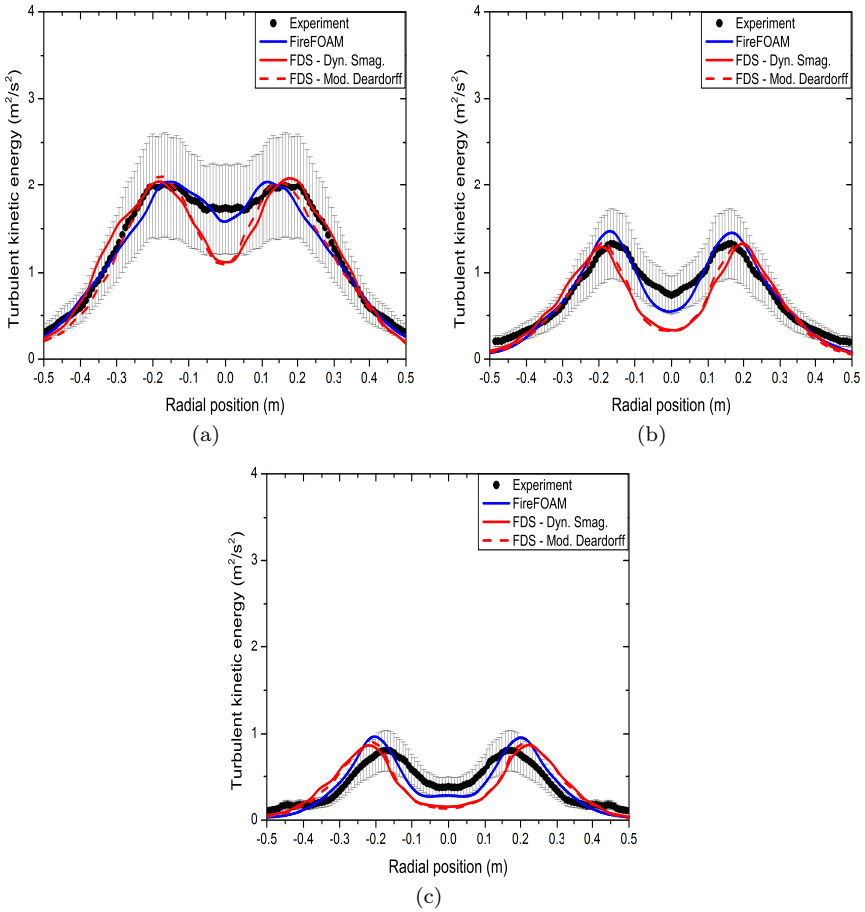

Fig. 14 Turbulent kinetic energies for Test #24 at height (a) $y = 0.9\ m$, (b) $y = 0.5\ m$ and (c) $y = 0.3\ m$.

to 2.61 MW (Test #17), even though it increases the air entrainment near the base of the fire plumes (see later), does not significantly alter the predicted frequencies in the numerical simulations. This is in line with what has been reported experimentally by Zukoski [43] and Cetegen [44]. Overall, the predicted puffing frequencies based on the axial velocity with both codes are in very good agreement with the (limited) experimental puffing frequencies reported by Tieszen et al. [12,13] but also with well-known correlations reported in literature. The predicted frequencies are also in good agreement with the experimental data by Pagni [45] (Figure 17) for a wide range of fire plumes, revealing an almost inversely linear relationship between the puffing frequency and the fire source diameter. The puffing frequencies based on temperature compare well with the experimental data and the experimental correlations for both the FireFOAM and the FDS simulations.

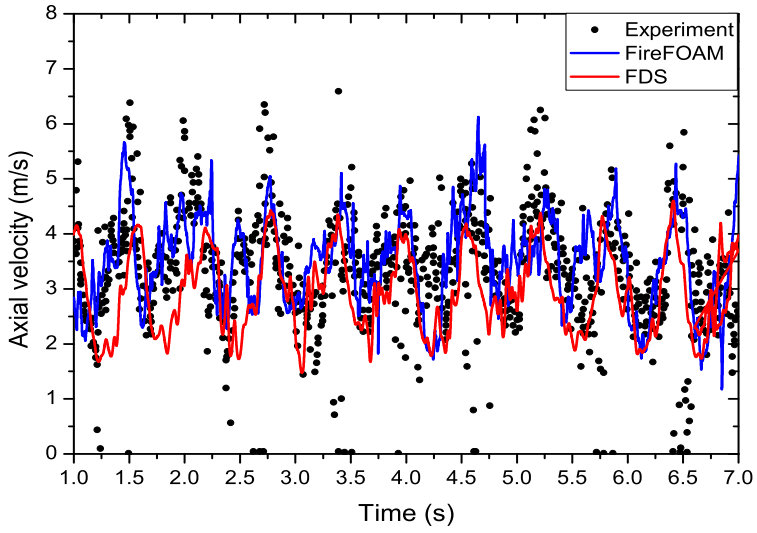

(a)

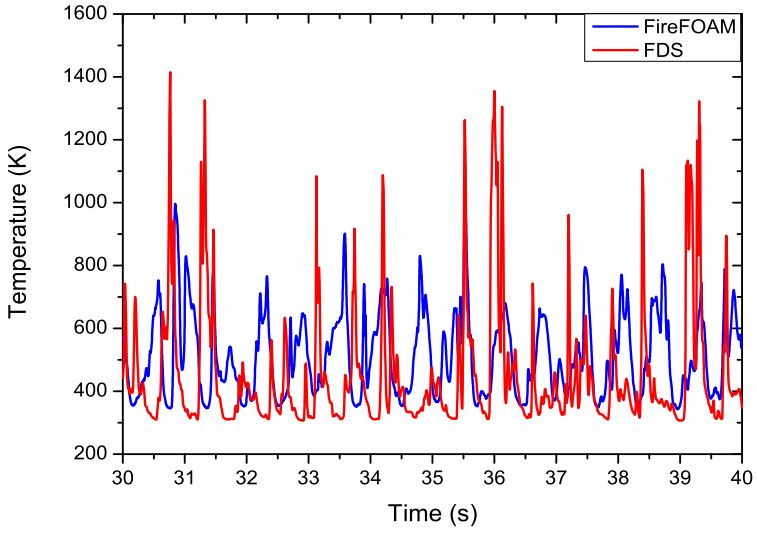

(b)

Fig. 15 Time trace at height $y = 0.5\ m$ for Test #17 of (a) axial velocity and (b) temperature.

Table 6 Predicted puffing frequencies based on axial velocity.

Test	Experiment (Hz)	Zukoski: Eq. (21) (Hz)	Cetegen: Eq. (22) (Hz)	FireFOAM (Hz)	FDS (Hz)
#14	-	1.57	1.50	1.58	1.69
#24	-	1.57	1.50	1.65	1.75
#17	1.65	1.57	1.50	1.66	1.64

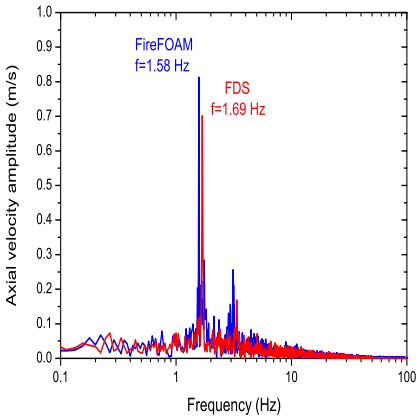

(a)

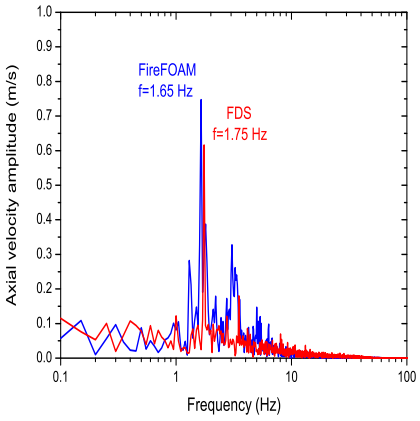

(b)

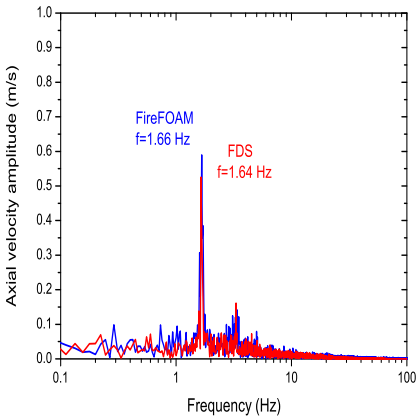

(c)

Fig. 16 Predicted amplitude spectrum of axial velocity at height $y = 0.5\ m$ for (a) Test #14, (b) Test #24 and (c) Test #17.

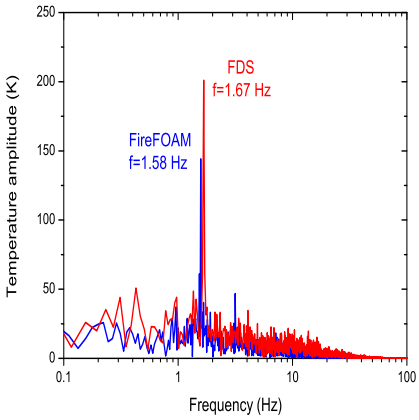

(a)

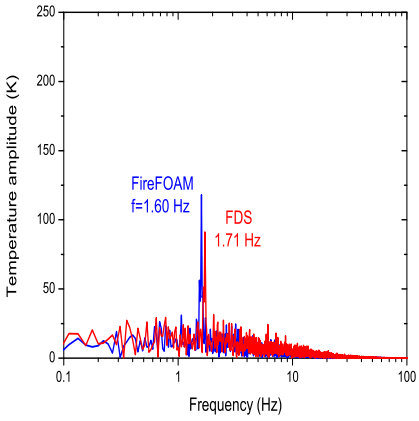

(b)

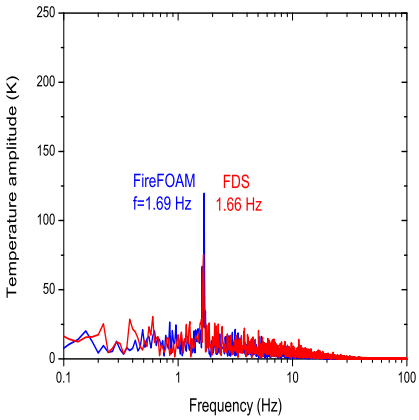

(c)

Fig. 17 Predicted amplitude spectrum of temperature at height $y = 0.5\ m$ for (a) Test #14, (b) Test #24 and (c) Test #17.

Table 7 Predicted puffing frequencies based on temperature.

Test	Experiment (Hz)	Zukoski: Eq. (21) (Hz)	Cetegen: Eq. (22) (Hz)	FireFOAM (Hz)	FDS (Hz)
#14	-	1.57	1.50	1.58	1.67
#24	-	1.57	1.50	1.60	1.71
#17	1.65	1.57	1.50	1.69	1.66

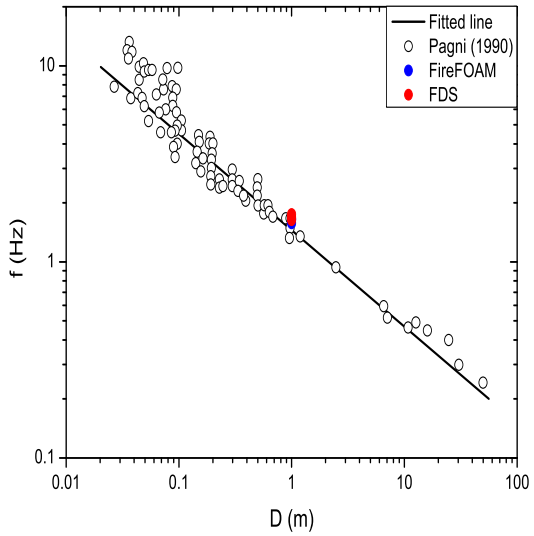

Fig. 18 Predicted puffing frequencies against experimental data from literature.

5.4 Flame height

Accurate prediction of flame height is in an important aspect for CFD codes since it can be important in cases related to flame spread such as, e.g., in external façades of buildings and areas involving combustible materials. The incident heat flux on a material surface is directly related to the predicted flame temperature by the CFD codes and the correct rate of pyrolysis of the material will strongly depend on the accurate prediction of the flame height in the numerical simulations.

An estimate of the flame height, L, for buoyant diffusion flames and pool fires has been given experimentally by Heskestad [46]:

$$\frac{L}{D} = 15.6N^{1/2} - 1.02 \tag{23}$$

where N is a non-dimensional number given by a modified Froude number [47]:

$$N = \frac{c_p T}{g\rho^2(\Delta Hc/s)^3}\frac{\dot{Q}^2}{D^5} \tag{24}$$

The predicted flame heights are presented in Table 8, along with the flame heights given by Heskestad's correlation (Eq. (23)). A common criterion to calculate the average flame height in numerical simulations is to determine the elevation

where there is a 500-600 K difference between the average flame temperature and the surrounding air temperature [36]. In the present study a temperature difference of 550 K was considered. The predicted flame heights by both codes, even though strongly dependent on the temperature criterion used to determine them, are generally in good agreement with Heskestad's correlation (±15%). The predicted flame heights also lie within the wide range of experimentally measured flame heights of different fuels and fire source sizes, presented in Figure 19, given as a function of the dimensionless heat release rate, Q^*, proposed by Zukoski [48]:

$$Q^* = \frac{\dot{Q}}{\rho_\infty c_p T_\infty (gD)^{1/2} D^2} \tag{25}$$

Table 8 Predicted flame heights based on the position on the centerline with $\Delta T = 550\ K$.

Test	Q*	Heskestad: Eq. (23) (m)	FireFOAM (m)	FDS (m)
#14	1.81	3.89	4.21	3.23
#24	2.34	4.48	4.86	4.08
#17	2.95	4.86	4.98	4.56

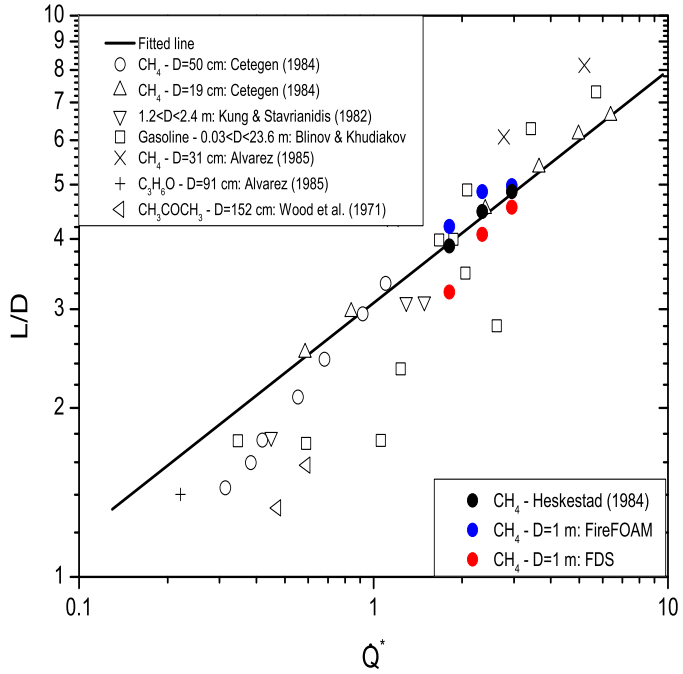

Fig. 19 Predicted flame heights, based on the position on the centerline with $\Delta T = 550\ K$, compared to experimental data from literature.

5.5 Entrainment

Accurate prediction of the air entrainment at different heights is another key element of capturing the dynamics and unsteady behavior of fire plumes in the numerical simulations. Air entrainment not only brings fresh air towards the reaction zone for the combustion to take place but also cools the combustion products while they are convected downstream from the fire source. Estimates of the entrainment rates in the flame, intermittent and plume region of fire plumes can be estimated based on Heskestad's experimental correlations [49]:

$$\dot{m} = \begin{cases} 0.0056\dot{Q}_c(y/L) & (y < L) \\ \\ 0.071\dot{Q}_c^{1/3}(y-y_0)^{5/3} + 1.92\times10^{-3}\dot{Q}_c & (y > L) \end{cases} \tag{26}$$

The predicted entrainment rates at different planes given by Heskestad's correlation (Eq. (26)) and the two codes are summarized in Table 9. In general, good agreement of the entrainment rates is evident with FireFOAM at almost all locations examined, except very high in the domain (close to the outlet plane of the domain). The entrainment rates with FDS are consistently lower, particularly in the intermittent and plume regions of the fire plumes.

Table 9 Predicted entrainments at different heights.

	Test #14			**Test #24**		
y (m)	Hesk.: Eq. (26) (kg/s)	FireFOAM (kg/s)	FDS (kg/s)	Hesk.: Eq. (26) (kg/s)	FireFOAM (kg/s)	FDS (kg/s)
0.5	0.92	1.28	1.02	1.04	1.31	1.08
1.0	1.83	2.34	1.76	2.07	2.39	1.84
2.0	3.66	4.28	3.12	4.14	4.40	3.27
3.0	5.49	6.09	4.54	6.21	6.31	4.73
4.0	8.46	7.91	6.14	8.28	8.26	6.35
5.0	11.66	9.91	7.84	12.58	10.40	8.03
6.0	15.37	12.09	8.80	16.54	12.64	9.04

	Test #17		
y (m)	Hesk.: Eq. (26) (kg/s)	FireFOAM (kg/s)	FDS (kg/s)
0.5	1.20	1.42	1.05
1.0	2.41	2.61	1.79
2.0	4.81	4.82	3.23
3.0	7.22	6.94	4.78
4.0	9.62	9.07	6.54
5.0	13.50	11.35	8.39
6.0	17.67	13.75	9.46

It is interesting to relate the entrainment rates with the predicted flame heights in the numerical simulations with the entrainment number, n, expressing the ratio of entrained air up to the flame tip with the stoichiometric air needed for complete combustion. Different values of the constant have been reported in literature; Tamanini [50] produced values of $n = 9$ based on numerical studies, Quintiere and

Grove [51] reported $n = 9.6$ for axi-symmetric and linear plumes, Delichatsios and Orloff [52] $n = 10$ for turbulent buoyant fires while Heskestad [53] and McCaffrey & Cox [54] values of $n = 12$. It is generally suggested that the entrainment number will have values of $n = 10 \pm 5$ at the flame tip [36]. Figure 20 presents the mass flow rates of Table 8 (excluding the mass flow rate of fuel at the source), normalized by the stoichiometric air required for complete combustion, and plotted against the axial location, non-dimensionalized by the predicted flame heights (previously presented in Table 7). Heskestad's correlation, with the entrainment number $n = 12$ at the flame tip, is also presented for comparative purposes. The results reveal that the entrainment rates predicted with both codes are linear. FireFOAM's entrainment number at the flame tip ($y/L = 1$) is $n = 12 - 15$ while for FDS is $n = 7 - 9$, both close to the reported values in literature.

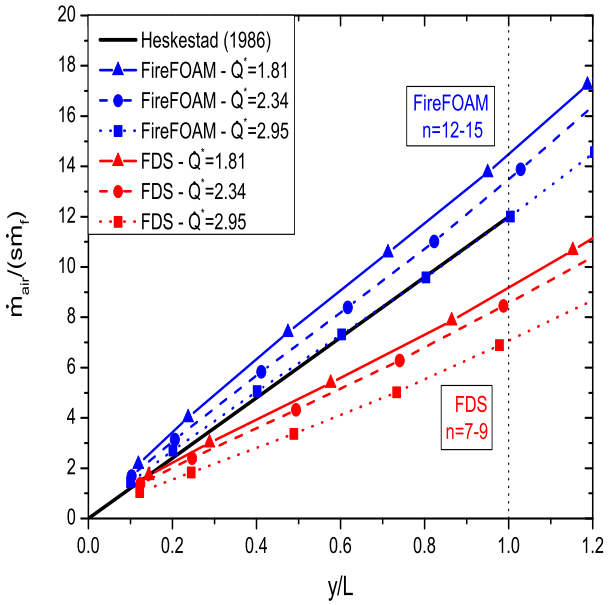

Fig. 20 Predicted air entrainment numbers at flame tip.

6 Grid sensitivity

In this section, a selection of results from a grid sensitivity analysis with both CFD codes is presented in Figures 21-23 for completeness of the current study. Results for the mean velocities and temperatures at height 0.9 m above the fire source and on the centerline with three different grid sizes (i.e. 1.5, 3.0 and 6.0 cm) for the three tests (i.e. #14, #24 and #17) are presented. It is very interesting to observe that the FDS results are not strongly grid dependent and comparable predictions are obtained with 1.5, 3.0 and 6.0 cm for both the velocities and temperatures at all the different locations examined. Similar behavior was observed for the FDS

results with the modified Deardorff on the same grid sizes (not shown here to avoid repetition). On the other hand, the FireFOAM results show a very strong grid dependency and reveal that relatively fine meshes ought to be used in the numerical simulations in order to have accurate predictions with the code. As expected, in both cases, the results with the finest grid employed (i.e. 1.5 cm) compare better with the experimental data.

The reasons for the observed differences can be attributed to a number of factors related to the modelling choices in the numerical simulations with FireFOAM. First, the Smagorinsky turbulence model constant, c_s, remains constant to 0.1 regardless the cell size employed in the simulations effectively making the fire plume more laminar as the cell size increases from 1.5 cm to 6 cm. On the other hand, the variation of the Smagorinsky constant on the coarser grids (i.e. 3 cm and 6 cm) with FDS exhibited similar behavior as the 1.5 cm cell size case, mostly remaining below 0.1 at heights up to $y = 1.0$ m and then increasing up to about 0.13. The variation of c_s with grid size in the FDS simulations is not presented here to avoid repetition, nevertheless, its evolution with axial position is similar to the one presented in Figure 11. This higher Smagorinsky coefficient in the FireFOAM simulations, results in more laminar-like structures at the base of the fire plumes which increases the predicted velocities and the flame temperatures on the centerline and results in the fire plume to break at distances much further downstream when compared to FDS. This is also confirmed by examining the rms values of temperature on the centerline on the coarse grids (i.e. 3 cm and 6 cm), presented in Figures 21(c), 22(c) and 23(c), which remain significantly lower with FireFOAM than with FDS and imply more laminar-like flame structures. Second, the resulting mixing time scales in FireFOAM remained consistently lower than FDS with increasing grid size (i.e. 3 cm and 6cm) very close to the fuel inlet similarly to what was reported in Figure 12 for a grid size of 1.5 cm. It is due to the different definition of τ_{turb} in FireFOAM and τ_u in FDS (or the different choice of constants in their derivation) that leads to significant differences between these two time scales and the resulting reaction rates and flame temperatures as well. Finally, a small contributing factor is attributed to the radiation modeling approach employed in FireFOAM which is grid-sensitive due to the dependence of the emission term of the RTI on the resolved temperature (i.e. T^4). The FDS results are less sensitive on this aspect due to the constant C employed in Eq. (13) which corrects the emission term based on a prescribed, by the user, global radiative fraction [22]. The resulting radiative fractions in the numerical simulations with the 1.5, 3 and 6 cm cell sizes were 24.8%, 28.3% and 25% for FireFOAM while 25.3%, 22.2% and 19% for FDS.

7 Conclusions

Large eddy simulations of large-scale CH_4 fire plumes with two different CFD packages, FireFOAM (version 2.2.x) and FDS (version 6.1.2), have been presented.

It was verified that the predominant mechanism for vorticity generation at the base of the fire source is due to the baroclinic and gravitational torques. However, with increasing axial distance from the fire source, only the influence of the baroclinic torque remains significant. In comparison to previously studied iso-thermal helium plumes [8,9], the non-monotonic behavior of density in the reaction zone of

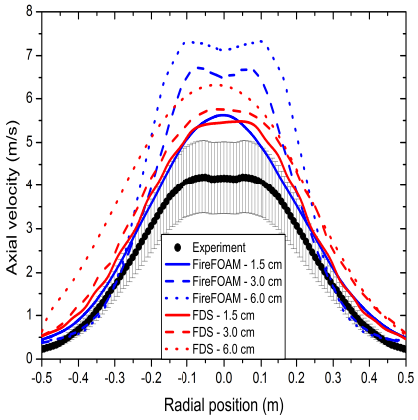

(a)

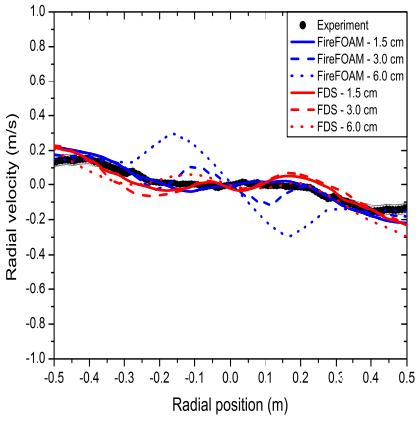

(b)

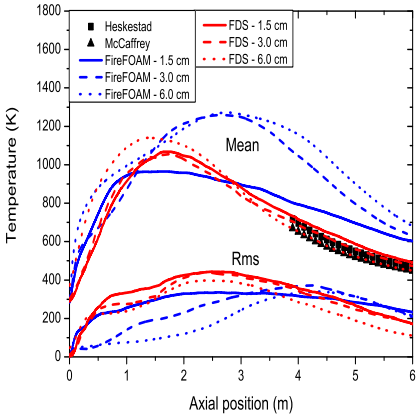

(c)

Fig. 21 Grid sensitivity for Test #14 on (a)axial velocities at height $y = 0.9\ m$, (b) radial velocities at height $y = 0.9\ m$ and (c) centerline temperatures.

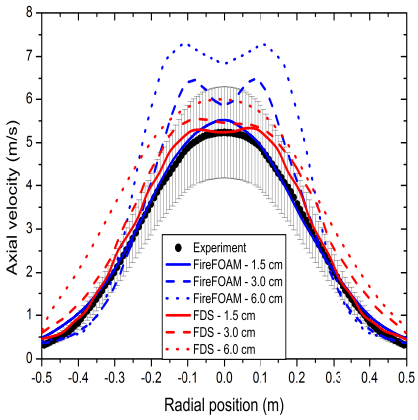

(a)

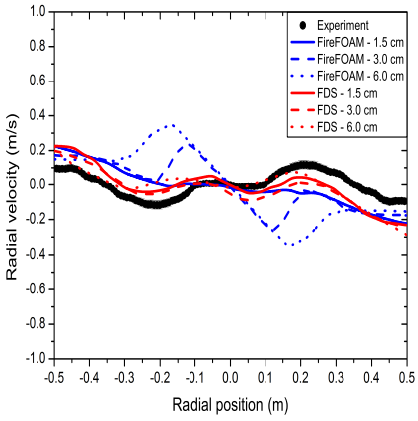

(b)

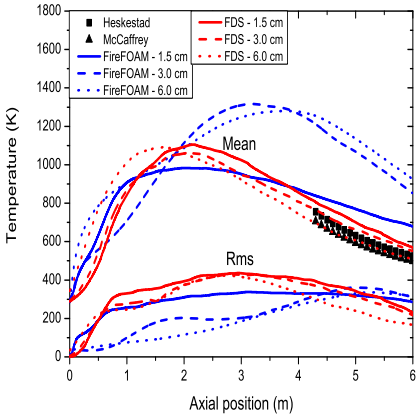

(c)

Fig. 22 Grid sensitivity for Test #24 on (a)axial velocities at height $y = 0.9\ m$, (b) radial velocities at height $y = 0.9\ m$ and (c) centerline temperatures.

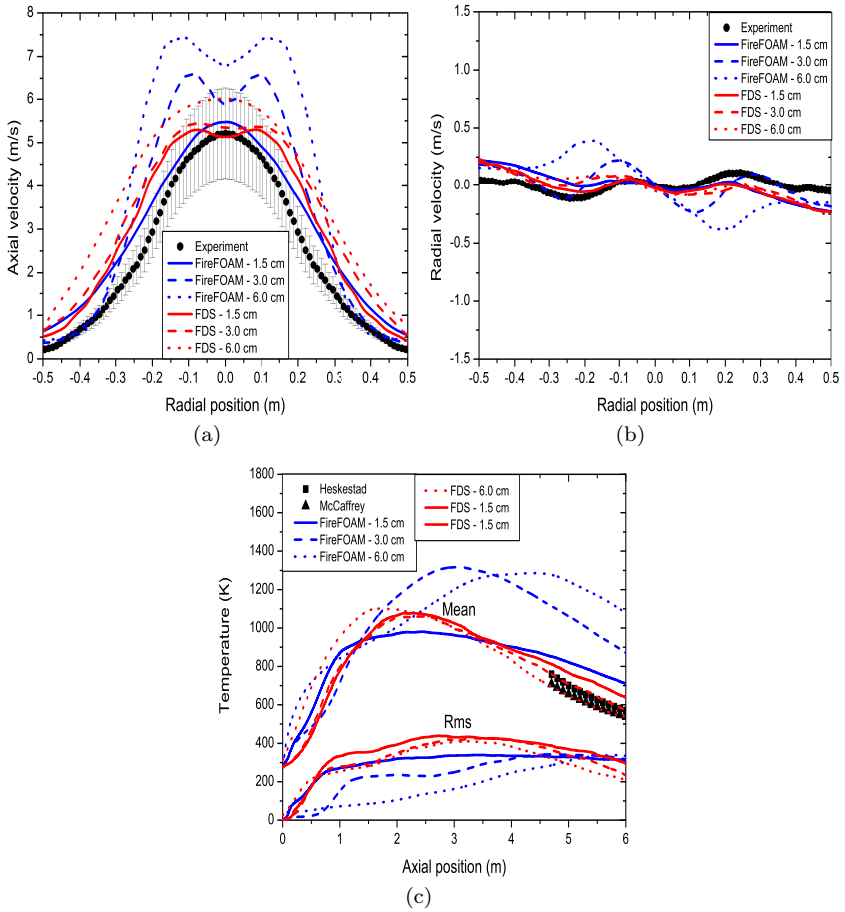

Fig. 23 Grid sensitivity for Test #17 on (a)axial velocities at height $y = 0.9\ m$, (b) radial velocities at height $y = 0.9\ m$ and (c) centerline temperatures.

these large-scale fire plumes is responsible for the creation of two counter-rotating vortices, enhancing the transport of fuel into the reaction zone [18].

There was, overall, good qualitative and quantitative agreement between the simulation results obtained with the two codes, but also with the experiments performed by Tieszen et al. [12,13] and well-known correlations reported in literature. The predicted mean and rms velocities and temperatures in the near-field region of the fire plumes, the average flame heights, entrainment rates, the puffing behavior, and resulting frequencies were well predicted and comparable between both codes. The main differences observed in the results obtained with the two codes were focused in the centerline mean and rms temperatures and entrainment rates. More specifically, FireFOAM over-predicted the temperatures in the plume region by approximately 100 K while almost no temperature fluctuation were evident with FDS. The differences observed in the centerline temperatures were attributed to the different reaction time scale models employed in the two codes which resulted in mixing time scales with FDS ($\tau_{mix} = 0.12\ s$) that were approximately double

those of FireFOAM ($\tau_{mix} = 0.056\ s$). This led to significantly higher reaction rates with FireFOAM in the flame and intermittent regions which resulted in hotter combustion products to be convected in the plume region. FDS consistently under-predicted the entrainment rates when compared to FireFOAM, particularly in the plume region where discrepancies of up to 45% were evident. The mean and rms results with FDS showed to be much less grid dependent than FireFOAM for mesh sizes of 1.5, 3.0 and 6.0 cm. The relatively strong grid dependency observed with FireFOAM poses a limitation when performing numerical simulations with the code since fine grid sizes need to be employed.

Updating some of the physical models of FireFOAM (i.e. related to turbulence, combustion and radiation) to the state-of-the-art modeling choices available in literature would improve the predictive capabilities of the code and enhance its range of applicability. The use of dynamic models for turbulence and combustion, where there is no possibility of pre-determination or calibration of the model constants, would be ideal and desirable.

References

1. B.J. Meacham, The evolution of performance based codes and fire safety design methods, National Institute of Standards and Technology, NIST-GCR-98-761 (1998)
2. G. Heskestad, Dynamics of the fire plume, Phil. Trans. R. Soc. Lond. A, 356, 2815-2833 (1998)
3. B.J. McCaffrey, Purely Buoyant Diffusion Flames: Some Experimental Results, NBSIR 79-1910, National Bureau Of Standards (1979)
4. E.E. Zukoski, T. Kubota, B. Cetegan, Entrainment in Fire Plumes, Fire Safety J., 3, 107-121 (1980)
5. B.M. Cetegen, E.E. Zukoski, T. Kubota, Entrainment and flame geometry of fire plumes, NBS-GCR 80-402, National Bureau of Standards, Gaithersburg, MD (1980)
6. P.H. Thomas, P.L. Hinkley, C.R. Theobald, D.L. Simms, Investigations into the flow of Hot Gases in Roof Venting, Fire Research Technical Paper no. 7, HMSO, London (1995)
7. A. Hamins, J.C. Yang, T. Kashiwagi, An Experimental Investigation of the Pulsation Frequency of Flames, Proc. Combust. Inst., 24, 1695-1702 (1992)
8. G. Maragkos, P. Rauwoens, Y. Wang, B. Merci, Large eddy simulations of the flow in the near-field region of a turbulent buoyant helium plume, Flow Turb. Combust., 90, 511-543 (2013)
9. P.E. DesJardin, T.J. O'Hern, S.R. Tieszen, Large eddy simulation and experimental measurements of the near-field of a large turbulent helium plume, Phys. Fluids, 16, 1866-1883 (2004)
10. G. Maragkos, B. Merci, Large Eddy Simulations of Large-scale CH_4 Fire Plumes, Proceedings of the 2^{nd} IAFSS European Symposium of Fire Safety Science (2015)
11. Y. Wang, P. Chatterjee, J.L. de Ris, Large eddy simulation of fire plumes, Proc. Comb. Inst., 33, 2473-2480 (2011)
12. S.R. Tieszen, T.J. O'Hern, E.J. Weckman, T.K. Blanchat, Experimental study of the flow field in and around a one meter diameter methane fire, Combust. Flame, 129, 378-391 (2002)
13. S.R. Tieszen, T.J. O'Hern, E.J. Weckman, R.W. Schefer, Experimental study of the effect of fuel mass flux on a 1-m diameter methane fire and comparison with a hydrogen fire, Combust. Flame, 139, 126-141 (2004)
14. B. Merci, J.L. Torero, A. Trouve, IAFSS Working Group on Measurement and Computation of Fire Phenomena, Fire Technol., 52, 607-610 (2016).
15. B. Merci, J.L. Torero, A. Trouve, Call for participation in the first workshop organized by the IAFSS Working Group on Measurement and Computation of Fire Phenomena, Fire Safety J., 82, 146-147 (2016).
16. S. Ferraris, J.X. Wen, S. Dembele, Large-eddy Simulation of a Large-scale Methane Pool Fire, Fire Safety Science, 8, 963-974 (2005)

17. A.R. Black, Numerical Predictions and Experiment Results for a 1m Diameter Methane Fire, ASME International Mechanical Engineering Congress and Exposition, 429-435 (2005)
18. P.E. DesJardin, Modeling of conditional dissipation rate for flamelet models with application to large eddy simulation of fire plumes, Combust. Sci. Technol., 177, 1883-1916 (2005)
19. Y. Xin, S.A. Filatyev, K. Biswas, J.P. Gore, R.G. Rehm, H.R. Baum, Fire dynamics simulations of a one-meter diameter methane fire, Combust. Flame, 153, 499-509 (2008)
20. H. Pasdarshahri, G. Heidarinejad, K. Mazaheri, Large eddy simulation on one-meter methane pool fire using one-equation sub-grid scale model, MCS 7, Chia Laguna, Cagliari, Sardinia, Italy, September 11-15 (2011)
21. M. Hu, A.C.Y. Yuen, S.C.P. Cheung, P. Lappas, W.K. Chow, G.H. Yeoh, Modelling of temporal combustion behaviour in a large-scale buoyant pool fire with detailed chemistry consideration, International Congress on Modelling and Simulation, Adelaide, Australia (2013)
22. K. McGrattan, S. Hostikka, R. McDermott, J. Floyd, C. Weinschenk, K. Overholt, Fire Dynamics Simulator Technical Reference Guide Volume 3: Validation, NIST Special Publication 1018-3, Sixth Edition (2015).
23. H. Jasak, A. Jemcov, Ž. Tuković, OpenFOAM: A C++ Library for Complex Physics Simulations, International Workshop on Coupled Methods in Numerical Dynamics IUC, Dubrovnik, Croatia, September 19^{th}-21^{st} (2007)
24. Z. Chen, J. Wen, B. Xu, S. Dembele, Large Eddy Simulation of Fire Dynamics with the Improved Eddy Dissipation Concept, Fire Safety Science, 10, 795-808 (2011)
25. N. Ren, Y. Wang, S. Vilfayeau, A. Truvé, Large eddy simulation of turbulent wall fires, 8^{th} U.S. National Combustion Meeting, Paper 070FR-0056 (2013)
26. K. McGrattan, S. Hostikka, R. McDermott, J. Floyd, C. Weinschenk, K. Overholt, Fire Dynamics Simulator Technical Reference Guide Volume 1: Mathematical model, NIST Special Publication 1018, Sixth Edition (2014)
27. J. Smagorinsky, General circulation experiments with the primitive equations: I. The basic experiment, Mon Weather Rev. 91, 99-164 (1963)
28. D.K. Lilly, A proposed modification of the Germano subgrid scale closure method, Phys. Fluids A, 4, 633-635 (1992)
29. J.W. Deardorff, Numerical Investigation of Neutral and Unstable Planetary Boundary Layers, Journal of Atmospheric Sciences, 29, 91-115 (1972)
30. S.B. Pope, Turbulent Flows, Cambridge University Press (2000)
31. B.F. Magnussen, B.H. Hjertager, On Mathematical Modeling of Turbulent Combustion with Special Emphasis on Soot Formation and Combustion, Proc. Comb. Inst., 16, 719-729 (1976)
32. R. McDermott, K. McGrattan, J. Floyd, A Simple Reaction Time Scale for Under-Resolved Fire Dynamics, Fire Safety Science, 10, 809-820 (2011).
33. C. Fureby, G. Tabor, Mathematical and Physical Constrains on Large-Eddy Simulations, Theoret. Comput. Fluid Dynamics, 9, 85-102 (1997)
34. W.L. Grosshandler, RADCAL: A Narrow-Band Model for Radiation Calculations in a Combustion Environment, NIST technical note 1402 (1993)
35. A. Hamins, T. Kashiwagi, R. Buch, Characteristics of pool fire burning, Fire resistance of industrial fluids, ASTM STP 1284, George E. Totten and Jurgen Reichel, Eds. American society for testing and materials, Philadelphia (1996)
36. D. Drysdale, An Introduction to Fire Dynamics, 3^{rd} Edition, John Wiley and Sons, England (2011)
37. K. McGrattan, J. Floyd, G. Forney, H. Baum, Improved radiation and combustion routines for a large eddy simulation fire model, Fire Safety Science, 7, 827-838 (2003)
38. NRC, Verification and Validation of Selected Fire Models for Nuclear Power Plant Applications, NUREG-1824, U.S. Nuclear Regulatory Commission, Washington D.C (2007)
39. W. Chung, C.B. Devaud, Buoyancy-corrected k- models and large eddy simulation applied to a large axisymmetric helium plume, International Journal of Numerical Methods in Fluids, 58, 57-89 (2008)
40. S.B. Pope, Ten questions concerning the large-eddy simulation of turbulent flows, New Journal of Physics, 6, 1-24 (2004)
41. I. Celik, M. Klein, J. Janicka, Assessment Measures for Engineering LES Applications, J. Fluids Eng., 131, 031102 (2009)
42. G. Heskestad, Engineering Relations for Fire Plumes, Fire Safety J., 7, 25-32 (1984)

43. E.E. Zukoski, Properties of fire plumes, Combustion Fundamentals of Fire (ed. G. Cox), 101-219, Academic Press, London (1983)
44. B.M. Cetegen, T.A. Ahmed, Experiments on the periodic instability of buoyant plumes and pool fires, Combust. Flame, 93, 157-184 (1993)
45. P.J. Pagni, Some unanswered questions in fluid mechanics, App. Mech. Rev., 43, 153-170 (1990)
46. G. Heskestad, Luminous heights of turbulent diffusion flames, Fire Safety J., 5, 109-114 (1983)
47. G. Heskestad, Peak gas velocities and flame heights of buoyancy-controlled turbulent diffusion flames, Proc. Comb. Inst., 18, 951-960 (1981)
48. E.E Zukoski, Convective Flows Associated with Room Fires, Semi Annual Progress Report, National Science Foundation Grant No. GI 31892 X1, Institute of Technology, Pasadena, CA (1975)
49. B. Karlsson, J.G. Quintiere, Enclosure Fire Dynamics, CRC Press (2000)
50. F. Tamanini, Reaction rates, air entrainment and radiation in turbulent fire plumes, Combust. Flame, 30, 85-101 (1977)
51. J.G. Quintiere, B.S. Grove, A unified analysis for fire plumes, Proc. Comb. Inst., 27, 2757-2766 (1998)
52. M.A. Delichatsios, L. Orloff, Entrainment measurements in turbulent buoyant jet flames and implications for modeling, Proc. Comb. Inst., 20, 267-375 (1984)
53. G. Heskestad, Fire plume air entrainment according to two competing assumptions, Proc. Comb. Inst., 21, 111-120 (1986)
54. B. McCaffrey, G. Cox, Entrainment and heat flux of buoyant diffusion flames, Report NBSIR 82-2473, National Bureau of Standards (1982)